Summer 2011

Two-step biodiesel production using supercritical methanol and ethanol

Ashley D'Ann Koh
University of Iowa

TWO-STEP BIODIESEL PRODUCTION USING SUPERCRITICAL METHANOL AND ETHANOL

by

Ashley D'Ann Koh

An Abstract

Of a thesis submitted in partial fulfillment
of the requirements for the Doctor of
Philosophy degree in Chemical and Biochemical Engineering
in the Graduate College of
The University of Iowa

July 2011

Thesis Supervisors: Adjunct Associate Professor Gary A. Aurand
Professor Gregory R. Carmichael

ABSTRACT

Current industrial biodiesel production utilizes an alkali catalyst that can participate in saponification side reactions. The side reactions are reduced by using highly refined vegetable oil feedstocks. Also, the catalyst must be extracted from the final product in a washing step. A catalyst-free alternative for the production of biodiesel was developed. It involves two reaction steps: 1) triglyceride hydrolysis (fat splitting) at subcritical conditions to separate glycerol from fatty acids, and 2) fatty acid esterification in supercritical alcohol to form fatty acid alkyl esters. The catalyst-free process can potentially be used with a variety of low-cost vegetable and animal fats without undesired side reactions.

The focus of this project was on the esterification reaction. Experiments were carried out with methanol and ethanol in a batch reaction system at supercritical conditions. High conversions could be attained at short reaction times. It was determined that the reaction followed second-order reversible kinetics. In addition, a novel Raman spectroscopic method was developed for the analysis of esterification reaction products.

Abstract Approved: _____
Thesis Supervisor

_____
Title and Department

_____
Date

_____
Thesis Supervisor

_____
Title and Department

_____
Date

TWO-STEP BIODIESEL PRODUCTION USING SUPERCRITICAL METHANOL AND ETHANOL

by

Ashley D'Ann Koh

A thesis submitted in partial fulfillment
of the requirements for the Doctor of
Philosophy degree in Chemical and Biochemical Engineering
in the Graduate College of
The University of Iowa

July 2011

Thesis Supervisors: Adjunct Associate Professor Gary A. Aurand
Professor Gregory R. Carmichael

Graduate College
The University of Iowa
Iowa City, Iowa

CERTIFICATE OF APPROVAL

PH.D. THESIS

This is to certify that the Ph.D. thesis of

Ashley D'Ann Koh

has been approved by the Examining Committee
for the thesis requirement for the Doctor of Philosophy
degree in Chemical and Biochemical Engineering at the July 2011 graduation.

Thesis Committee: _____
Gary A. Aurand, Thesis Supervisor

_____
Gregory R. Carmichael, Thesis Supervisor

_____
Julie L. P. Jessop

_____
David G. Rethwisch

_____
Horacio F. Olivo

To CMC

ACKNOWLEDGMENTS

I would like to thank my thesis advisor, Dr. Gary A. Aurand, for giving me the opportunity to work on this project and for guiding me through its completion. I am thankful to the Iowa Energy Center for funding this project. I would also like to thank my thesis committee members for their valuable suggestions for this project. I am grateful to Dr. Gregory R. Carmichael for providing funding support for my poster presentation at the ACS Spring 2010 National Meeting. I especially want to thank Dr. Julie L. P. Jessop for helping me in the development of the Raman spectroscopic analytical method and for her mentorship.

I appreciate all the help that I received from the Aurand research group, especially Taiying Zhang, Kehinde Bankole, and all the undergraduate research assistants that have worked with me. I would like to thank Peter Hatch at the Glass Shop and Frank Turner at the Machine Shop for fabricating materials for my experiments. Special thanks to Linda C. Wheatley and Natalie J. Potter for ensuring that I met all my deadlines on time.

Not in the least, I would like to thank my family and friends for their love and support. I want to thank the Angels, Sherrie R. Elzey and Jessica Rodriguez-Navarro, for sharing my laughs and tears. Most of all, I owe this accomplishment to the loving support of my husband, Christopher M. Comer.

TABLE OF CONTENTS

LIST OF TABLES

LIST OF FIGURES

CHAPTER 1

INTRODUCTION

The demand for energy derived from biorenewable resources is ever-increasing due to the volatility of oil prices and mounting concerns over energy security and climate change. Biodiesel, an alternative fuel derived from vegetable oil, has been gaining popularity in recent years, as shown in Figure 1.[1]

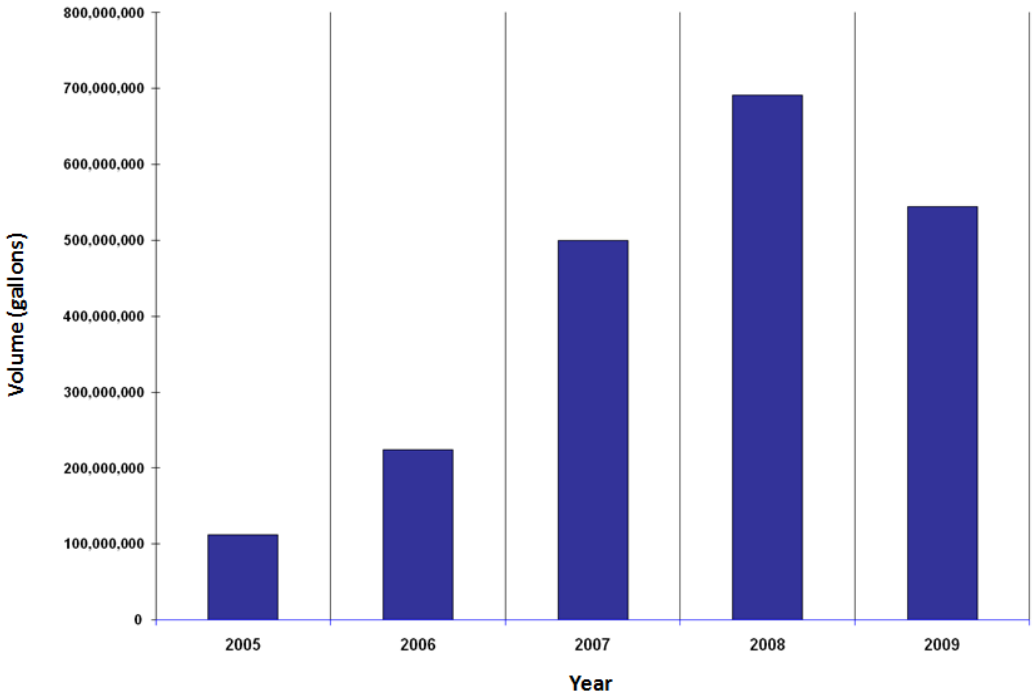

Figure 1. Estimated U.S. biodiesel production by calendar year.[1]

In the United States, soybean oil is the most common feedstock for biodiesel production.[2] Biodiesel is a critical component in the shift to biofuels because it is compatible with existing diesel engines (compression ignition engines) without the need for any modifications,[3] and production technology is immediately available.

However, current biodiesel production technology requires the use of a corrosive liquid catalyst that is very sensitive to the quality of the feed oil. This catalyst is susceptible to the production of unwanted by-products that can congest reactors and cause production downtime. Consequently, highly refined oil must be used and this increases production costs. Thus, to address this prevailing issue, a non-catalytic method for the production of biodiesel was investigated in this study. Further background information on current industrial biodiesel production will be discussed in the next chapter, as well as the current state of research on the use of sub- and supercritical fluids in biodiesel production. The specific objectives of this project will be outlined in Chapter 3 and the results of each portion of the project will be presented in subsequent chapters.

CHAPTER 2

BACKGROUND

2.1. Conventional Biodiesel Production

Conventional biodiesel production uses the transesterification reaction, with the aid of a catalyst, to produce biodiesel. The reaction is shown in Figure 2. Triacylglycerols of oil react with an aliphatic alcohol, typically methanol since it is cheapest, in the presence of a catalyst. The most common catalysts used are alkaline, namely, sodium methoxide, sodium hydroxide, or potassium hydroxide. The products of the reaction are fatty acid alkyl esters, otherwise known as biodiesel, and glycerol.

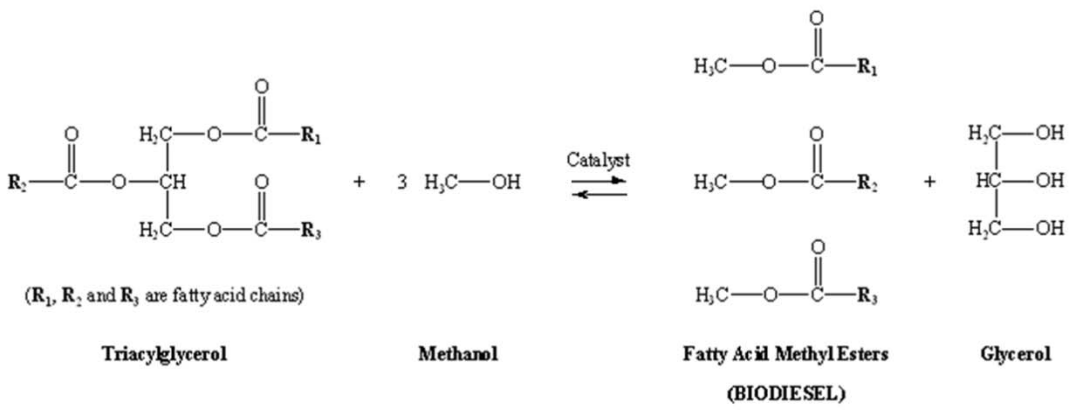

Figure 2. Transesterification reaction used in conventional biodiesel production.

Figure 3 presents a generic process flow diagram of commercial biodiesel production.[4] Since transesterification is a reversible reaction, excess alcohol is used to drive the reaction forward. Van Gerpen et al.[5] reported that 60–100% excess methanol is generally used to make sure that the reaction reaches completion. The reaction also requires about 1% (based on the weight of oil) of the base catalyst that ultimately ends up

in the glycerol layer of the products. Sometimes, a second transesterification reaction is performed, after removal of glycerol, to maximize biodiesel yield.

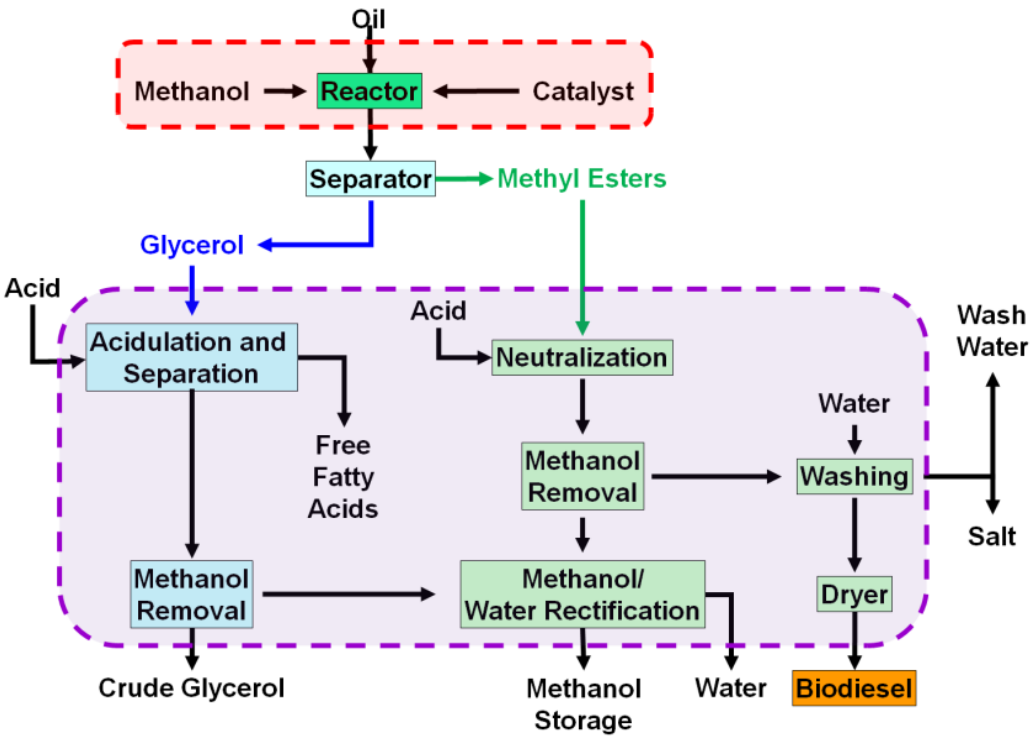

Figure 3. Conventional biodiesel production flow diagram.[4]

The reaction time depends on the molar ratio of alcohol to oil and the temperature of the reaction. In Figure 4, Freedman et al.[6] showed that 98% conversion to soybean oil methyl esters can be obtained in 1 hour when using a 6:1 molar ratio at a temperature of 60 °C.

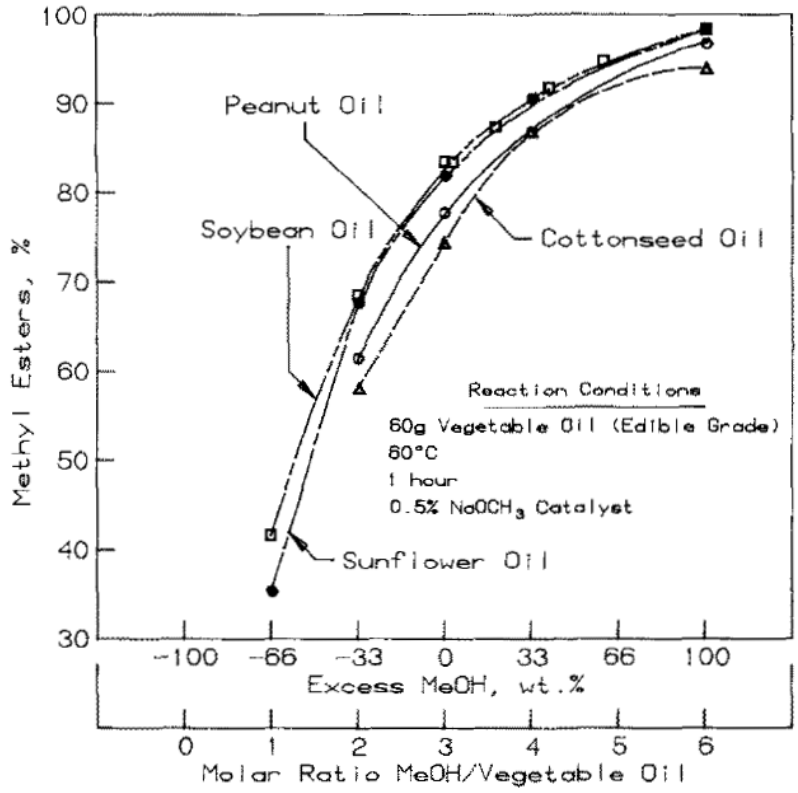

Figure 4. Effect of molar ratio of alcohol to oil on methyl ester yields.[6]

The biodiesel product and glycerol co-product streams require a significant number of refining steps, shown within the bottom dotted box in Figure 3. At least 25% of the equipment costs is associated with these steps, according to a process model that estimates these costs for a 10 million gal/year facility.[7]

Furthermore, the quality of the feed oil in this process must be low in moisture, phosphorus, and fatty acids to attain higher process yields and prevent the formation of undesired by-products, particularly soap, which would result in additional refining steps. Thus, highly refined feedstock, such as refined bleached deodorized (RBD) oil is used and it is the most expensive raw material, accounting for 88% of the total annual operating costs.[7] Thus, to overcome these issues associated with the use of this catalyst, a non-catalytic method using supercritical alcohols was explored in this research.

2.2 Supercritical Fluids

Supercritical fluids (SCFs) possess unique solvent properties that allow them to be used in various industrial applications. The most widely known application is in the decaffeination of coffee.[8] More recently, SCFs have been used as benign solvents in various production stages in the microelectronics,[9] pharmaceutical,[10, 11] biomedical,[12] and biofuels[13] industries.

To better understand what SCFs are, the generalized phase diagram of a pure substance in Figure 5 will aid in the visualization of the concepts presented. The critical point is located at the upper end of the vapor pressure curve. At this point, the distinction between liquid and gas disappears.[14] Table 1 lists the critical properties of some common solvents.

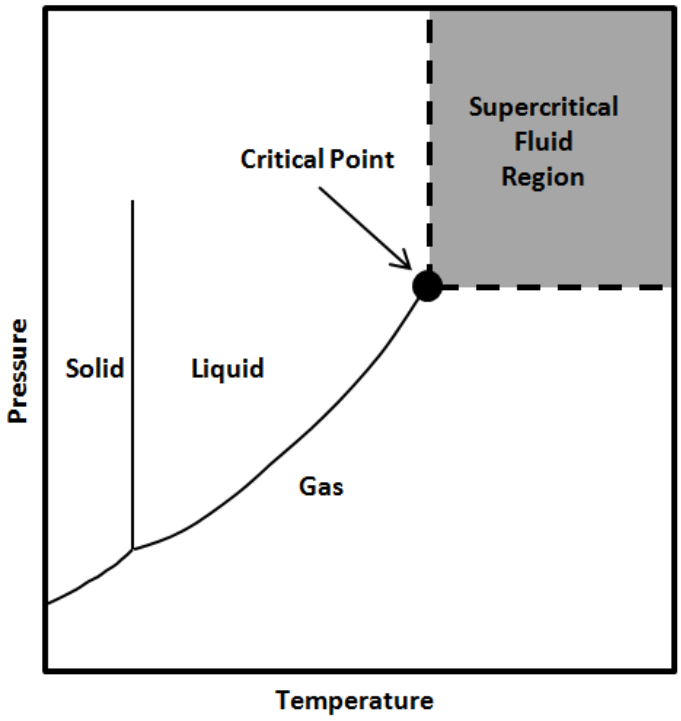

Figure 5. Phase diagram of a pure substance.

Table 1. Critical data for select substances.[15]

Substance Name	Molecular Weight	Critical Temperature (K)	Critical Pressure (bar)	Critical Density (g/cm^3)
Methanol	32.042	512.58	80.96	0.2720
Ethanol	46.069	516.25	63.84	0.2760
Water	18.015	647.13	220.55	0.3220
Carbon dioxide	44.010	304.19	73.82	0.4682

At conditions above the critical point (i.e., critical temperature and pressure), the fluid exists in a supercritical phase where it exhibits properties that are in between those of a liquid and a gas. More specifically, SCFs have a liquid-like density and gas-like transport properties (i.e., diffusivity and viscosity). This can be seen in Table 2, wherein the typical values of these properties are compared between the three fluids. Moreover, the dissolving power of SCFs can be adjusted by manipulating temperature and pressure.

Table 2. Comparison of typical physical property values for liquids, SCFs, and gases.[16]

Property	Liquid	SCF	Gas
Density (g/mL)	1	0.3	10^{-3}
Diffusivity (cm^2/s)	5×10^{-6}	10^{-3}	0.1
Viscosity (Pa·s)	10^{-3}	10^{-4}	10^{-5}

The numerous advantages to using SCFs in chemical synthesis are summarized in Jessop and Leitner's book on the topic.[17] Environmentally, most substances that are used as SCFs do not contribute to smog nor do they damage the ozone layer. Carbon dioxide and water, specifically, pose no acute ecotoxicity. Also, no liquid waste is produced by carbon dioxide and other volatile SCFs. In addition to their environmental benefits, most SCFs are noncarcinogenic and nontoxic. All these benefits combined with their unique

chemical properties make SCFs an attractive alternative to address the current need to use green solvents that are more environmentally friendly.

2.3. Non-Catalytic Transesterification

To minimize the downstream refining steps associated with the conventional biodiesel production process, Diasakou et al.[18] investigated the thermal non-catalytic transesterification of soybean oil with methanol. Reactions were carried out at temperatures below the critical temperature of methanol (240 °C), at 220 °C and 235 °C, in a batch stirred tank reactor. Since then, several researchers have continued to study the sub- and supercritical transesterification of various seed oils. Pinnarat and Savage[19] have reviewed the studies that have been published to date. Table 3 below is adapted from their summary.

Table 3. Summary of non-catalytic transesterification studies.[19]

Authors	Year	Oil Type	Temperature, Pressure	Molar Ratio (Alcohol:Oil)	Reaction Time	Reactor Type	Conversion
Saka and Kusdiana[20]	2001	rapeseed	350 °C, 450 bar	42:1	4 min	5 mL Inconel-625	95%
Demirbas[21]	2002	hazelnut kernel	350 °C	41:1	5 min	100 mL cylindrical autoclave SS	95%
Madras et al.[22]	2004	sunflower	350 °C, 200 bar	40:1	40 min	8 mL reactor SS	96%
Bunyakiat et al.[23]	2006	coconut, palm kernel	350 °C, 190 bar	42:1	7 min	tubular flow reactor SS	95%
He et al.[24]	2007	soybean	280 °C, 250 bar	42:1	30 min	200 mL reactor	90%
He et al.[25]	2007	soybean soybean	310 °C, 350 bar 100−320 °C (gradually heat)	40:1 40:1	25 min 25 min	75 mL tube reactor 75 mL tube reactor	77% 96%
Silva et al.[26]	2007	soybean (ethanol)	350 °C, 200 bar	40:1	15 min	24 and 42 mL tubular reactor SS	80%
Demirbas[27]	2008	cottonseed (methanol) cottonseed (ethanol)	230 °C 230 °C	41:1 41:1	8 min 8 min	cylindrical autoclave SS cylindrical autoclave SS	98% 75%

Several of these studies attempted to model the kinetics of the reaction. Diasakou et al.[18] applied the model of a three-step reaction mechanism wherein the triacylglycerol is broken down into a diacylglycerol then a monoacylglycerol before fully liberating the glycerol as shown below:

$$\text{Triacylglycerol} + \text{Methanol} \rightarrow \text{Diacylglycerol} + \text{Fatty Acid Methyl Ester} \quad (1)$$

$$\text{Diacylglycerol} + \text{Methanol} \rightarrow \text{Monoacylglycerol} + \text{Fatty Acid Methyl Ester} \quad (2)$$

$$\text{Monoacylglycerol} + \text{Methanol} \rightarrow \text{Glycerol} + \text{Fatty Acid Methyl Ester} \quad (3)$$

It was assumed that each step was irreversible due to the high molar ratio of alcohol to oil used. Also, each step was assumed to be of first order with respect to each reacting component. The experimental data was in agreement with the calculated values.

Other kinetic studies[22, 24, 26, 28] used a simplified model consisting only of the overall reaction, as shown below:

$$\text{Triacylglycerol} + 3\text{Methanol} \rightarrow \text{Glycerol} + 3\text{Fatty Acid Methyl Esters} \quad (4)$$

Once again, the reaction was assumed to be irreversible due to the high molar ratio of alcohol to oil used and it was also assumed to be first order in the triacylglycerol.

Kusdiana and Saka[28] observed a discontinuity between the two linear regions in the Arrhenius plot, the subcritical region at low temperature and the supercritical region at high temperature, as shown in Figure 6. He et al.[24] also observed a similar discontinuity in the non-catalytic transesterification of soybean oil in methanol. This discontinuity could be attributed to the critical point of the reaction mixture. The separate linear region at temperatures below this point could be limited by methanol solubility at low temperatures.[29]

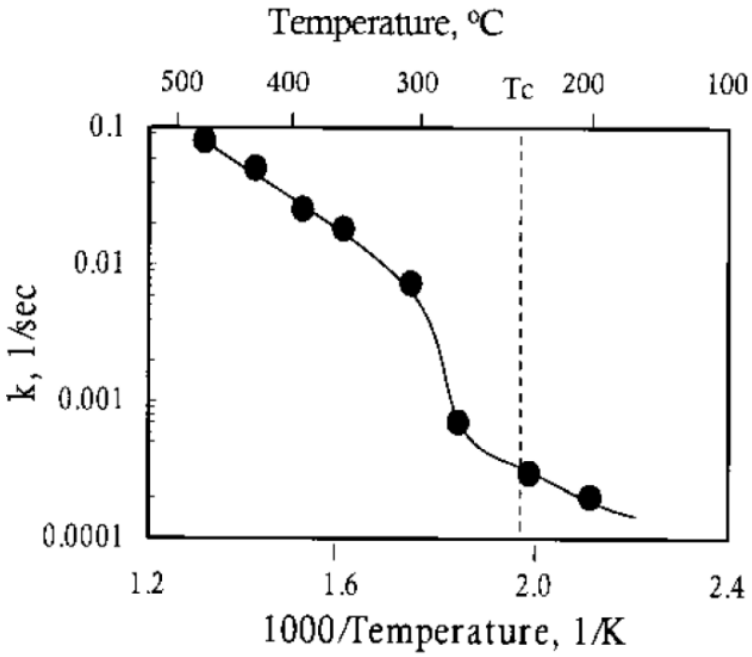

Figure 6. Arrhenius plot of the non-catalytic transesterification of rapeseed oil in methanol, where: Tc = critical temperature of methanol (240 °C).[28]

A wide range of activation energies were reported due to the variability of reaction conditions across studies. Conflicting reports[30, 31] currently exist on the effect of unsaturated fatty acids on the reaction rate. Furthermore, Dasari et al.[29] suggest that the metal surfaces of the reactor could increase the reaction rate. Thus, more research is needed to fully understand the effects of each of the different variables on the kinetics of non-catalytic transesterification.[19]

2.4. Non-Catalytic Two-Step Process

High reaction temperatures and molar ratios of alcohol to oil are required for the non-catalytic transesterification of seed oils to biodiesel. Kusdiana and Saka[28] determined the optimum temperature for this process to be 350 °C while maintaining a molar ratio of 42:1 (alcohol to oil). It is an energy intensive process, particularly with respect to the methanol recycle loop.[32] Hence, to lower these reaction conditions, Kusdiana and Saka[33]

suggested a two-step non-catalytic process. First, a hydrolysis step, performed under subcritical water conditions, splits the fatty acids from the glycerol backbone of the triacylglycerol. Second, the free fatty acids are esterified with supercritical methanol to produce biodiesel. The process flow diagram is shown in Figure 7.

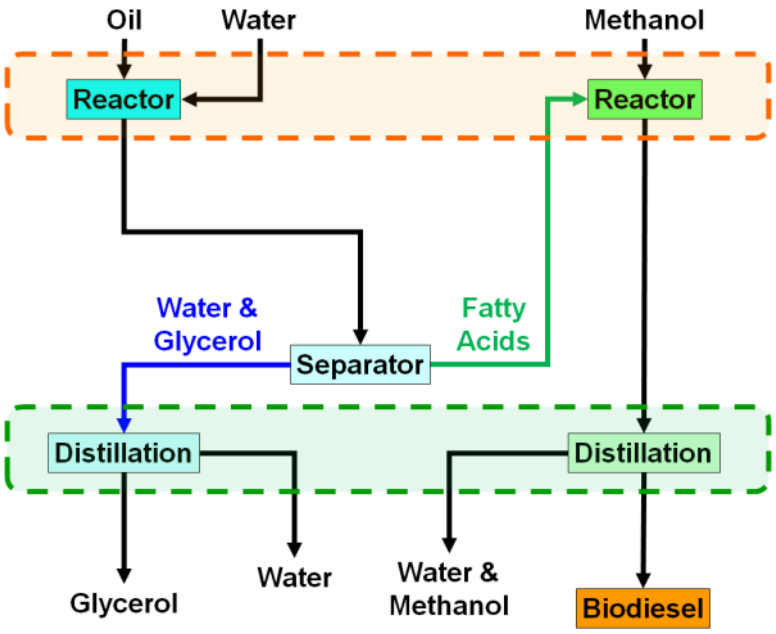

Figure 7. Two-step non-catalytic production of biodiesel.[33]

In contrast to conventional biodiesel production using a homogeneous catalyst, this process has fewer post-reaction refining steps. The reduction in the number of production steps could provide significant cost savings. Also, less waste would be produced since there is no catalyst involved.

2.4.1. Subcritical Hydrolysis

The hydrothermal hydrolysis of triacylglycerols is a mature process that dates all the way back to 1854.[34] Since then, several processes have been developed,[35] namely, the Twitchell process,[36] the Colgate-Emery synthesis,[37] and the Eisenlohr process.[38]

The Colgate- Emery synthesis is still the predominantly used process in industry today for the splitting of fats and oils.[39] Typical operating conditions for this process are 250 °C and 5.07 MPa. Under these conditions, a 2 hour reaction can yield 97% fatty acids.[40] However, since the oil to water ratio is 2:1, it is regarded more as a steam-based process than a subcritical one.[41] Thus, Holliday et al.[41] and King et al.[35] studied hydrolysis reactions under sub- and supercritical conditions where the density is more liquid-like (>0.5 g/mL).

Using a tubular flow reactor, King et al.[35] could achieve 90–100% yields of free fatty acids at 330 °C to 340 °C and oil to water ratios of 1:2.5 and 1:5 in short residence times (10–15 min). Furthermore, the reactor system was equipped with a view cell, allowing for the observation of the phase change during the reaction. The reaction mixture became a single phase at 339 °C, indicating the complete miscibility of the oil and water.

It was our aim to use subcritical hydrolysis of soybean oil to generate free fatty acids that would subsequently be used in esterification experiments. The capacity of an existing continuous flow microreactor system in the Aurand research laboratory was evaluated for use in this process.

2.4.2. Supercritical Esterification

The esterification of fatty acids is typically carried out with the use of acid catalysts.[42, 43] The earliest documentation of the use of high temperatures and pressures for these types of reactions includes a number of patents for the production of rosin acid esters.[44-46] Few papers have been published on the esterification of fatty acids exclusively with sub- and supercritical alcohols for the purposes of producing biodiesel.[33, 47-51] Some studies have also looked into non-catalytic esterification in tandem with solid acid catalysts.[52-54]

Compared to non-catalytic transesterification, non-catalytic esterification of fatty acids can be performed at lower temperatures and pressures, as well as with lower molar ratios of alcohol to fatty acids. Most of the studies cited above have focused on temperatures between 250 °C and 320 °C. Figure 8 shows the effect of temperature on the yield of methyl esters obtained from non-catalytic esterification and non-catalytic transesterification reactions that were conducted under the same conditions.[48] Looking at the data trend for 320 °C, a 90% yield of methyl ester can be obtained for the non-catalytic methyl esterification of oleic acid in less than 10 minutes. On the other hand, the non-catalytic transesterification of rapeseed oil only yielded 30% methyl esters in the same amount of time. Moreover, even after 30 minutes reaction time, only a 65% yield was obtained. Thus, esterification occurs much more rapidly than transesterification at lower temperatures.

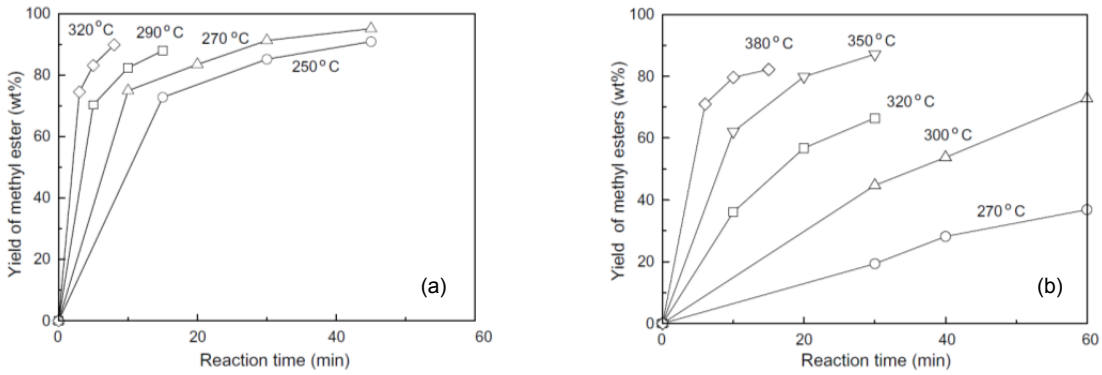

Figure 8. Effect of temperature on the yield of methyl esters at 20 MPa (from Minami and Saka[48]): (a) methyl esterification of oleic acid, and (b) transesterification of rapeseed oil. Both reactions were carried out with a volumetric ratio of alcohol to fatty acid or triacylglcreol of 1.8:1.

Similarly, the molar ratio of alcohol to fatty acid affects the yield of methyl ester in the same way that temperature does. This can be seen in Figure 9 showing the yield of methyl esters for different molar ratios used in both non-catalytic esterification and

transesterification reactions. Remarkably, for non-catalytic esterification, a high yield of methyl ester (>90%) was obtained using a molar ratio of only 3:1. A tenfold increase in molar ratio is required for non-catalytic transesterification to achieve the same yield. Hence, non-catalytic esterification utilizes less alcohol and can provide significant cost savings in terms of raw material consumption and energy usage for recovery.

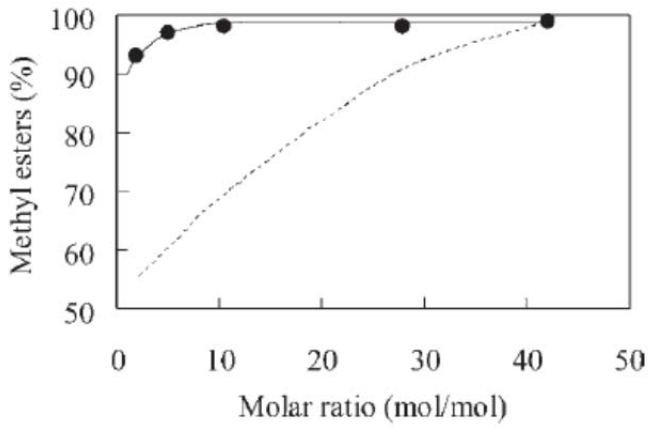

Figure 9. Effect of the molar ratio of methanol to oleic acid on the yield of methyl esters at 270 °C and 10 minutes.[33] The dashed line represents data for transesterification (from Kusdiana and Saka[28]).

Since non-catalytic esterification for biodiesel production is a recent innovation, there is a lack of information on the kinetics of the reaction. Minami and Saka[48] studied the kinetics for both the hydrolysis and esterification steps in the two-step process developed by Kusdiana and Saka.[33] Tubular flow reactors, made of Hastelloy C-276, were used in their study and they employed an autocatalytic reaction mechanism to model both reactions. The esterification reaction sequence is shown below:

$$\text{Fatty Acid} \rightleftarrows \text{Fatty Acid}^- + H^+ \text{ (dissociation of Fatty Acid)} \quad (5)$$

$$\text{Fatty Acid} + H^+ \rightleftarrows \text{Fatty Acid}^+ \text{ (protonation of Fatty Acid)} \quad (6)$$

$$\text{Fatty Acid}^{+} + \text{Methanol} \rightleftarrows \text{Fatty Acid Methyl Ester}^{+} + \text{Water (methyl esterification)} \quad (7)$$

$$\text{Fatty Acid Methyl Ester}^{+} \rightleftarrows \text{Fatty Acid Methyl Ester} + H^{+} \text{ (deprotonation)} \quad (8)$$

In the first step, a fatty acid is dissociated to release a hydrogen ion (a proton). This is followed by the protonation of the carbonyl oxygen of the fatty acid. Alcohol then attacks the protonated carbonyl group, and a protonated ester is formed upon the release of a water molecule. A final proton transfer yields the fatty acid methyl ester. Figure 10 compares this model with the experimental data. The theoretical values calculated using the model appear to agree with the experimental data. However, neither the calculated reaction rate constants nor the activation energies were reported.

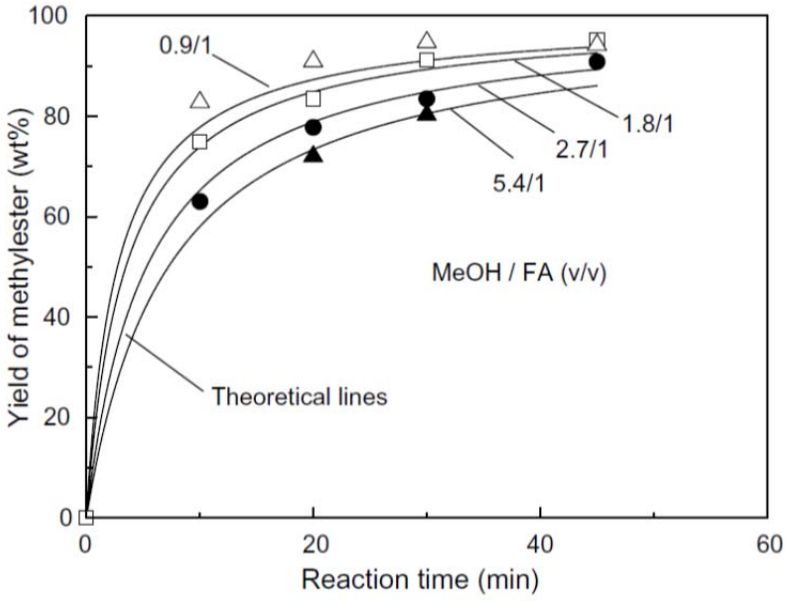

Figure 10. Comparison of the theoretical yields calculated from the autocatalytic model and experimental data for esterification reactions at 270 °C and 20 MPa at various volumetric ratios of methanol to oleic acid.[48]

Alenezi et al.[51] investigated the esterification of a mixture of fatty acids, predominantly oleic acid (88%), with supercritical methanol in a batch stirred-tank reactor made of stainless steel. They used a one-step reversible reaction scheme:

$$\text{Fatty Acid} + \text{Alcohol} \rightleftarrows \text{Fatty Acid Methyl Ester} + \text{Water} \quad (9)$$

They found that this reversible second order reaction model fit their data, as shown in Figure 11. The rate constants of the forward and reverse reactions were found using non-linear optimization. An Arrhenius plot, as shown in Figure 12, was generated to obtain the activation energies of the reactions. All the kinetic parameters calculated are shown in Table 4.

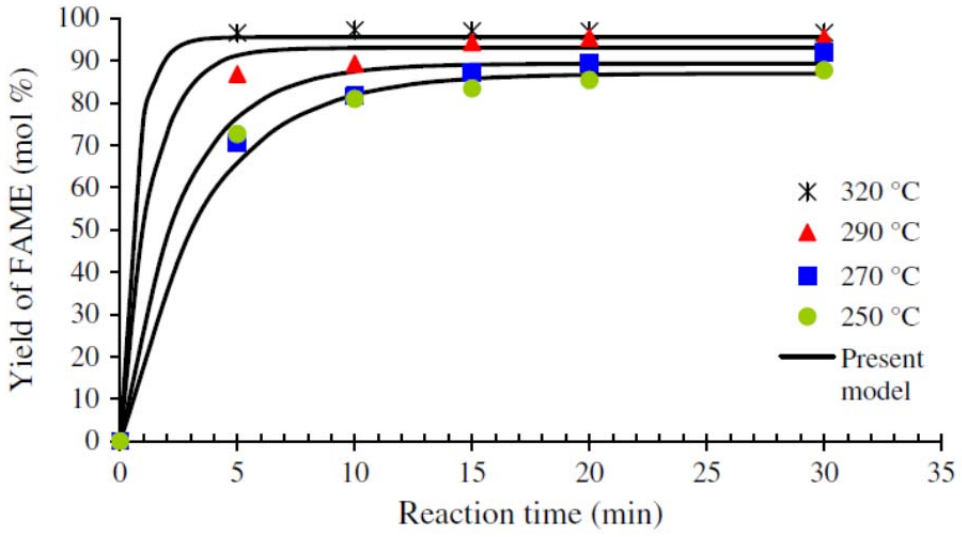

Figure 11. Effect of temperature on the yield of methyl esters at 10 MPa, 430 rpm and molar ratio of methanol to FFA of 7:1.[51]

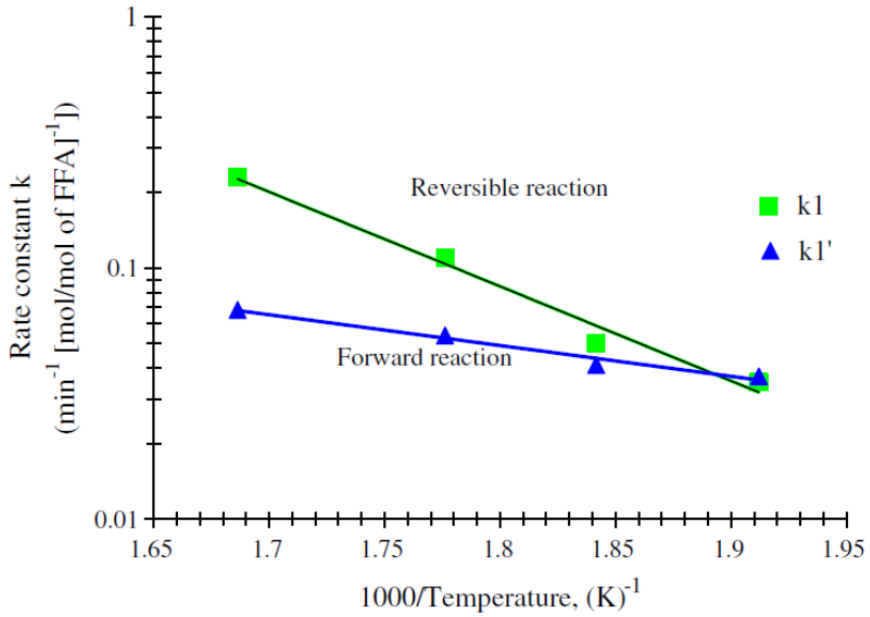

Figure 12. Arrhenius plot for the esterification of fatty acids in supercritical methanol.[51]

Table 4. Kinetic parameters for esterification (molar ratio of methanol to FFA = 7:1).[51]

Temperature	**k_1 (min^{-1}[mol/mol of fatty acid]$^{-1}$)**	**k_{-1} (min^{-1}[mol/mol of fatty acid]$^{-1}$)**
250 °C	0.035	0.037
270 °C	0.050	0.054
290 °C	0.110	0.054
320 °C	0.230	0.063
R^2	0.98	0.97
Pre-exponential factor (A)	5.0×10^5 min^{-1}[mol/mol of fatty acid]$^{-1}$	7.9 min^{-1}[mol/mol of fatty acid]$^{-1}$
Activation energy (Ea)	72 kJ/mol	23.2 kJ/mol

Pinnarat and Savage[50] also used this reversible second order reaction model to determine the kinetics of the esterification of oleic acid in sub- and supercritical ethanol. Ethanol was used in their reactions because it can be derived from biomass and limited research has been done with this alcohol.[55] Additionally, biodiesel properties (e.g. cloud point) could potentially be improved through the use of longer chain alcohols.[56]

They primarily used quartz batch reactors to eliminate any potential catalytic effects from the use of a metal reactor. However, their comparison with 316 stainless steel reactors showed minimal differences in yield between the two reactor materials used.

They also looked into the effect of phase behavior on the kinetics of the reaction. Process simulation software, ASPEN Plus version 2006.5, was used to perform vapor-liquid calculations to estimate the reaction pressure and the composition and amount of each phase present in the reactor. Figure 13 shows the agreement between the model and their experimental data for single-phase reactions at low temperatures (liquid) and high temperatures (supercritical). The Arrhenius plot is shown in Figure 14 and the all the kinetic parameters determined from the model and the plot are tabulated in Table 5.

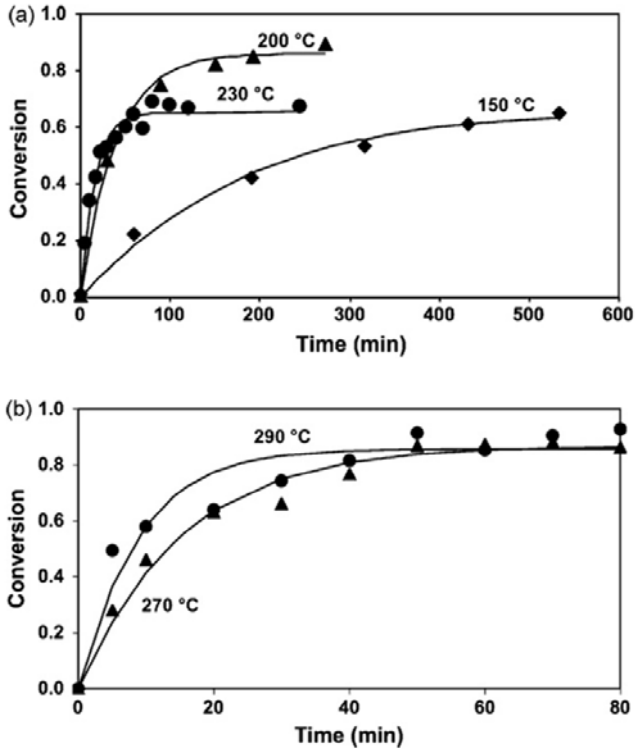

Figure 13. Fit of the reversible second order reaction model with experimental data (from Pinnarat and Savage[50]): (a) liquid phase (low temperature), and (b) supercritical phase.

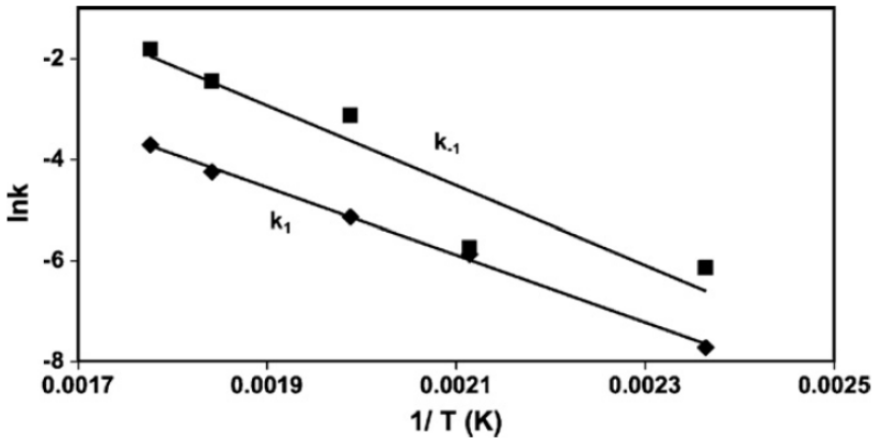

Figure 14. Arrhenius plot for the forward and reverse reactions.[50]

Table 5. Calculated kinetic parameters for the reversible second order reaction model.[50]

Temperature	Volumetric filling factor	Ethanol:Oleic acid molar ratio	k_1 (L mol^{-1} min^{-1})	k_{-1} (L mol^{-1} min^{-1})
150 °C	0.80	7:1	(4.5 ± 1.1)E−04	(2.2 ± 1.6)E−03
200 °C	0.80	7:1	(2.8 ± 0.6)E−03	(3.2 ± 1.9)E−03
230 °C	0.56	10:1	(5.9 ± 0.8)E−03	(4.4 ± 1.1)E−02
270 °C	0.26	35:1	(1.4 ± 0.3)E−02	(8.7 ± 5.9)E−02
290 °C	0.26	35:1	(2.4 ± 1)E−02	(1.6 ± 1.6)E−01

This model was also tested on two-phase reactions, however the model underpredicted the conversions. Further work is required in understanding the thermodynamics, transport phenomena (especially in varying reactor configurations), and reaction kinetics for the esterification of fatty acids in sub- and supercritical alcohols in order to design an economically feasible process.

Given the dearth of research in this area, it was our objective to investigate the kinetics of esterification of linoleic acid, which is the main component of soybean oil, in supercritical methanol and ethanol. Experiments at various temperatures and reaction

times were conducted and several kinetic models were investigated to determine the best fit to the data.

2.5. Analytical Methods

The numerous methods used in biodiesel analysis have been reviewed by Knothe[57] and recently updated by Monteiro et al.[58] Gas chromatography (GC) is the most common method for determining biodiesel produced from transesterification. However, this method requires sample derivatization that does not allow the simultaneous detection of free fatty acids and their alkyl esters. Thus, it is not applicable for the analysis of esterification reaction products.

Titration is a method that has been reported in some papers to determine the conversion of free fatty acids to esters.[52, 59, 60] Based on standard specifications such as the American Oil Chemists' Society (AOCS) official method Cd 3d-63,[61] the acid values of the feed and product are used in a simple calculation to determine conversion. However, this method requires sample volumes that are too large for products from experiments carried out in microreactor systems.

Spectroscopic methods can readily characterize both carboxylic acid and ester products[62] and they also have been studied for their application in biodiesel reaction monitoring.[58] Ghesti et al.[63] used Raman spectroscopy to quantify transesterification reaction products by comparing the differences in several bands of the vegetable oil and ethyl ester spectra. They also successfully correlated their results with several Nuclear Magnetic Resonance (NMR) methods.[64] Raman spectroscopy is a non-destructive method of analysis and it can be used in real-time, in-line monitoring of reactions, even in microreactors.[65] Due to these features and the availability of the instrument, a Raman spectroscopic method was developed for the analysis of reaction products from the esterification of fatty acids.

CHAPTER 3

OBJECTIVES

The overall aim of this research was to develop an environmentally friendly and economical method of producing biodiesel under sub- and supercritical conditions by first hydrolyzing oil to obtain free fatty acids and then esterifying the free fatty acids to produce the alkyl esters. Since the hydrolysis of fats and oils is a mature industrial technology, focus was placed on the esterification reaction. The kinetics of the reaction were of particular interest because it provides information that is essential in reactor design and scale-up. It also allowed for the comparison with conventional catalytic biodiesel production. Thus, the specific objectives of this research were:

- To develop a Raman spectroscopic analytical method to measure the extent of reaction for methyl and ethyl esterification.
- To determine the effect of temperature, reaction time, and alcohol on the conversion of the esterification reaction.
- To develop an accurate reaction model that predicts the progress of the esterification reaction at short (<10 min) and long reaction times (>10 min).

First, a Raman spectroscopic method was developed for the analysis of the esterification products since it did not require any sample modification, and spectral data could be obtained from small sample volumes. A calibration curve was developed with the use of prepared solutions that simulated the progress of the esterification reaction. It was validated by predicting the reaction conversion of samples with known concentrations before use in the analysis of actual reaction products generated from experiments.

Second, esterification reactions were carried out in a batch reactor at various temperatures and reaction times. Two alcohols were investigated in this study: 1) methanol, a low cost alcohol most commonly used in commercial biodiesel production,

and 2) ethanol, a biorenewable solvent. Experiments conducted at short reaction times (<10 min) were of particular interest in this study since previous research had not explored this time range.

Third, a search for a kinetic model that best fit the data collected from the esterification experiments was conducted. Reaction rate constants were determined for both methyl and ethyl esterification. Arrhenius plots were also generated to calculate the activation energy and pre-exponential factor for each reaction.

CHAPTER 4
EXPERIMENTAL STUDY OF HYDROLYSIS REACTIONS IN FLOW REACTOR SYSTEMS

The use of flow type reactors are of great interest in the study of reactions in sub- and supercritical media because they provide the ability to control the pressure of the reaction system. Bench-scale experiments in these systems also allow for future scale-up design for industrial applications. Hydrolysis reactions were performed in these systems to verify previous research and to generate free fatty acids to be used in subsequent esterification experiments.

4.1. Reactor Configurations

Two types of flow reactor configurations were investigated in this study: 1) a microreactor, and 2) a tubular reactor. Findings on the use of each type of reactor are discussed in detail in the sections below.

4.1.1. Continuous Flow Microreactor System

The microreactor setup was first investigated for its use in hydrolysis experiments. A schematic diagram of the reactor system is shown in Figure 15. Water was pumped, using an HPLC pump (LabAlliance, State College, PA), through a tube furnace (Thermolyne 79400, Thermo Fisher Scientific Inc., Waltham, MA) to preheat it to the desired reaction temperature. Soybean oil (Hy-Vee Inc., West Des Moines, IA) was pumped, using another HPLC pump (LabAlliance, State College, PA), directly into the microreactor (High Pressure Equipment Co., Erie, PA) where it came into contact with the preheated water. The microreactor was constructed of 316 stainless steel and had a reaction volume of 0.17 ml. A thermocouple (Omega Engineering Inc., Stamford, CT) was placed at the center of the reaction zone to monitor the reaction temperature. A heat exchanger at the end of the reaction zone quenched the reaction products. The pressure of

the reaction system was controlled by a back pressure regulator (Tescom Corp., Elk River, MN) located at the end of the heat exchanger.

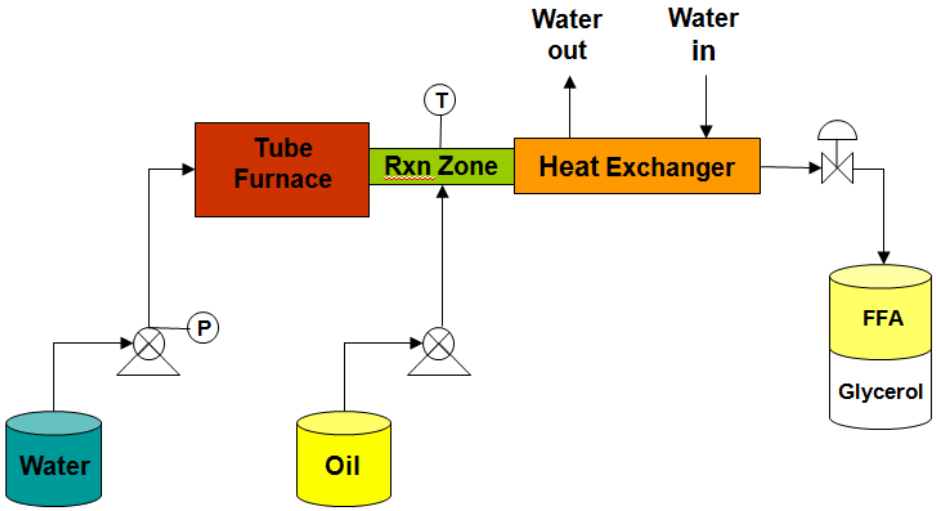

Figure 15. Continuous flow microreactor system.

Preliminary experiments to determine the feasibility of this system for hydrolysis reactions were conducted using the optimum conditions, established by Kusdiana and Saka,[33] to obtain complete conversion of oil to free fatty acids. The reaction temperature was set at 270 °C and the pressure of the system was maintained at 7.85 MPa. Also, the molar ratio of oil to water used for the reaction was 1:4.

The reaction product consisted of two layers: 1) a clear yellow top layer that contained the fatty acids and unreacted oil, and 2) an opaque white bottom layer that contained water, glycerol, mono-, and diacylglycerols. Centrifugation facilitated a more efficient separation of the top and bottom layers. Titration was used, following the AOCS official method Ca 5-40,[66] to determine the conversion to free fatty acids. Very low conversions (<1%) were obtained, indicating that the residence time of the reactants in the reaction zone was too short. Thus, the reaction zone needed to be expanded to

increase conversion. A new flow reactor system was designed and is discussed in the next section.

4.1.2. Tubular Reactor System

In order to increase the conversion of the hydrolysis reaction, a tubular reactor with a larger reaction zone volume was designed. A schematic diagram of the new reactor is shown in Figure 16. The reaction zone consisted of a 6.1 m long, 3.86 mm I.D. stainless steel tube (Swagelok Co., Rock Island, IL) bent into an accordion shape so that it would fit inside a fluidized sand bath (Techne Inc., Burlington, NJ). The calculated volume of the reaction zone was 70 ml. Two thermocouples were placed inside the reaction zone, one at each end of the zone, so that the temperature of the reaction could be monitored accurately. The feed lines into the reaction zone were preheated with a heating tape (Thermo Fisher Scientific Inc., Waltham, MA).

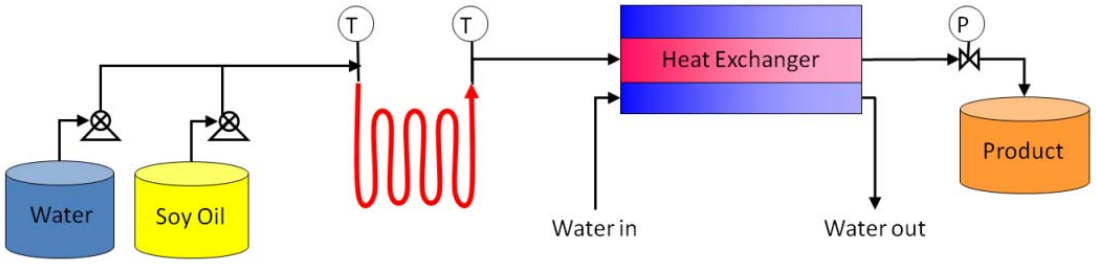

Figure 16. Continuous flow reactor system.

Two sets of hydrolysis experiments were performed using this reactor setup: 1) flow rate runs, and 2) temperature runs. For the flow rate runs, reactions were carried out at different pump flow rates to study the effect of varying residence times on the conversion of oil to free fatty acids. Soybean oil (Hy-Vee Inc., West Des Moines, IA) was used and the volumetric ratio of oil to water used was 1:1, based on the ratio used by

Minami and Saka[48] in their kinetics study. Temperature was held constant at 270 °C. One set of flow rate runs was carried out at 10 MPa while another set was carried out at 13.1 MPa. This was done to see the effect of pressure on the reaction. Each run was performed in triplicate. The results are shown in Figure 17. It can be seen that higher conversions can be attained at shorter reaction times at higher pressures.

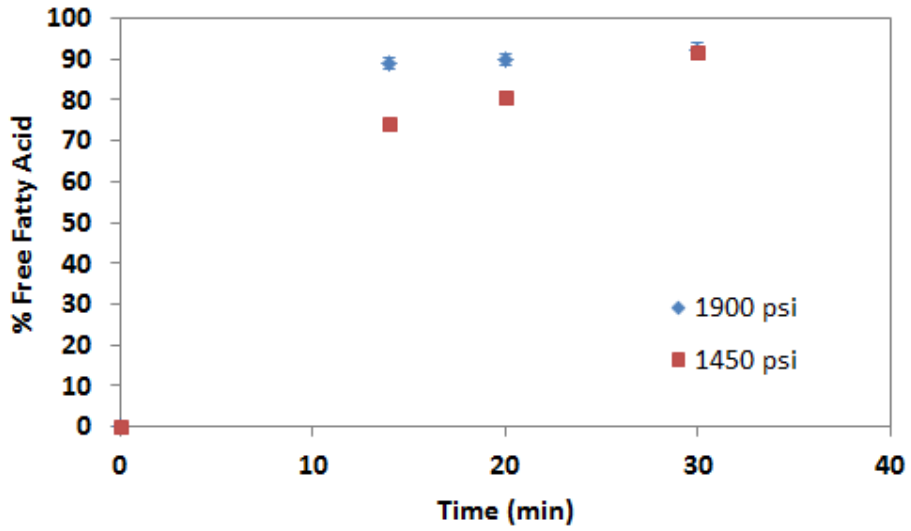

Figure 17. Effect of pressure and varying residence times on the conversion of oil to free fatty acids.

For the temperature runs, soybean oil was again used as well as the volumetric ratio of oil to water of 1:1. Pressure was held constant at 10 MPa. The residence time of the reaction was 14 minutes. Each run was performed in triplicate. The results are shown in Figure 18 and it can be seen that they are comparable to the results of Minami and Saka.[48]

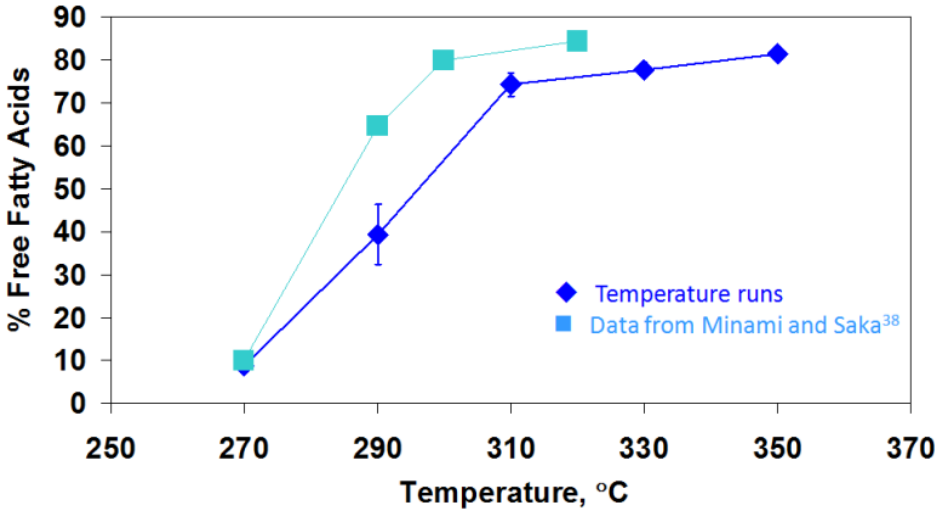

Figure 18. Effect of temperature on the conversion of oil to free fatty acids. The lines are present to aid in trend visualization.

Further experimentation to expand the data set for the temperature runs (i.e. perform experiments at different residence times) was suspended due to repeated clogging of the back pressure regulator that resulted in equipment failure. Thus, in-house production of free fatty acids was discontinued and the fatty acids for the esterification experiments were purchased.

4.2. Survey of Analytical Methods for Hydrolysis and Esterification

Titration was selected for use in determining the conversion of the hydrolysis reaction because it was a simple and efficient analytical method that could be performed without the need for highly specialized equipment. The free fatty acid content in the hydrolysis reaction product was determined using AOCS official method Ca 5-40.[66]

To supplement the conversion results obtained by the use of titration, other analytical methods were surveyed to provide additional information about the extent of

the reaction such as product component profiles. This survey was conducted simultaneously with the work on the tubular reactor.

4.2.1. Gas Chromatography-Mass Spectrometry

Gas chromatography-mass spectrometry (GC-MS) was initially evaluated as a method to obtain a comprehensive component profile of the hydrolysis reaction product since it is a common method used by lipid researchers. The instrument used in the High Resolution Mass Spectrometry Facility at the University of Iowa was a Thermo Voyager single quadrupole mass spectrometer (Thermo Fisher Scientific Inc., Waltham, MA). However, it was determined that the configuration of the system was not ideal for the purposes of this research. Therefore, an alternative analytical method was sought out.

4.2.2. Thin-Layer Chromatography

Thin-layer chromatography (TLC) was investigated as a quick, low-cost method to determine the presence of partially reacted components (i.e. diglycerides and monoglycerides) in the hydrolysis reaction product. TLC can be used to separate classes of lipids on a TLC plate based on their differing solubility in the developing solvent and adsorption to the plate. An example of a typical separation scheme for simple lipids can be seen in Figure 19.[67]

Figure 19. Example of a separation of a vegetal lipid after lipid hydrolysis, where: TG = triacylglycerols, 1,3-DAG = 1,3-diacylglycerols, 1,2-DAG = 1,2-diacylglycerols, FFA = free fatty acids, 2-MG = 2-monoacylglycerols, and 1-MG = 1-monacylglycerols.[67]

A method was developed based on a simple recipe to separate lipid mixtures.[68] First, a suitable developing solvent for the samples had to be prepared from a mixture of different solvents. After trial and error experiments with several formulations, a hexane/ether/acetic acid mixture (70/30/1, v/v) was chosen for use in the separation of the components in the hydrolysis reaction product.

TLC plates were spotted with the samples and then developed using the solvent in a covered glass jar. After drying, the plates were placed under an ultraviolet (UV) light in order to see the individual fractions as spots on the plate. The spots were difficult to see at first. This problem was resolved with the use of primuline, a fluorescent dye that makes the spots more prominent under UV light. However, with the termination of the hydrolysis experiments, verification of the results from this TLC method was also halted.

4.2.3. Nuclear Magnetic Resonance

Proton nuclear magnetic resonance (^{1}H-NMR) spectroscopy was explored for the analysis of esterification reaction products. A Bruker DRX-400 with a BBO broadband probe (Bruker Biospin Corp., Billerica, MA) located at the Central NMR Research Facility at the University of Iowa was used to obtain the spectra of the samples.

Each of the individual components of the esterification reaction, as well as the esterification reaction products, were diluted in chloroform-d (Sigma-Aldrich, St. Louis, MO) using a volumetric ratio of sample to chloroform of 1:5 and then analyzed. It was observed that the NMR signal of the methanol hydroxyl group overlapped with the signal of the methyl ester protons. Removal of excess methanol from the reaction products could have resolved this issue, however solvent removal was not feasible for the small sample volumes used during experiments. Thus, the use of this method was not further pursued.

4.3. Summary

In summary, two different flow reactor configurations were assessed for use in hydrolysis experiments. The microreactor volume was too small for the purposes of generating free fatty acids for the subsequent esterification reaction. Thus, a plug flow reactor system with a larger reaction zone was designed and assembled. This reactor system yielded promising preliminary results. However, due to repeated equipment failure, work on this system was discontinued. Additionally, several methods were

surveyed for the analysis of the hydrolysis reaction product. Titration provided basic information about the extent of reaction while TLC could provide supplementary information about the composition of the reaction product. Furthermore, NMR was investigated for the analysis of esterification reaction products. Overlapping NMR signals of the methanol hydroxyl group and the methyl ester protons deemed this method unsuitable for the needs of this research.

CHAPTER 5
DEVELOPMENT OF RAMAN SPECTROSCOPIC ANALYTICAL METHOD

Several analytical methods were reviewed for the analysis of the reaction products in this research. In the previous chapter, it was mentioned that GC-MS was investigated as a method for the analysis of hydrolysis reaction products. During that survey, it was also examined for use in the analysis of esterification reaction products. It was determined that the problems that hindered its use for hydrolysis also applied to esterification. Additionally, GC methods require sample derivatization that transforms carboxylic acids to esters before analysis. Hence, the unreacted acids would not be distinguished from the esters formed during experiments. NMR was also investigated for its use as a method to determine reaction conversion. However, removal of excess alcohol used in the esterification reaction would have been necessary. Due to the small sample sizes used in this research, this method was not feasible.

To circumvent the issues associated with the use of the methods mentioned above, Raman spectroscopy, a light-scattering technique, was investigated as a method for the analysis of esterification reaction products. Raman scattering is the inelastic scattering of a molecule, wherein the excited molecule relaxes to a different vibrational state.[69] This is exhibited by a change in the frequency (wavelength) of the light, providing important chemical information. The method does not require any sample modifications or any special sample holders. Thus, this method has potential application in in-line reaction monitoring. The details of the development of this analytical method are discussed in the following sections.

5.1. Materials and Methods

5.1.1. Materials

Linoleic acid, methyl linoleate, and ethyl linoleate (Sigma-Aldrich, St. Louis, MO), along with methanol (Fisher Scientific, Fair Lawn, NJ) and ethanol (AAPER Alcohol and Chemical Co., Shelbyville, KY), were used to create standard mixtures to simulate the reaction products of methyl and ethyl esterification. All materials were used as received.

5.1.2. Experimental Method

A Raman spectroscopic system, consisting of a HoloLab 5000R modular research Raman spectrograph, an Mk II filtered probehead, and an Invictus 785 nm near-infrared laser (Kaiser Optical Systems Inc., Ann Arbor, MI), was used to collect the Raman spectra of the samples. The power output of the laser was set at 200 mW. The samples were placed in a quartz microcuvette (PerkinElmer Inc., Waltham, MA) and exposed to the laser for 1 second for 3 accumulations. Each sample was analyzed in triplicate. All measurements were acquired with auto-dark subtraction and cosmic ray correction.

5.2. Results and Discussion

Five standard mixtures of linoleic acid, ester, and alcohol were prepared to simulate the progression of the reaction. The concentrations of these mixtures are listed in Table 6. Methyl linoleate and methanol were used to characterize the reaction products of methyl esterification while ethyl linoleate and ethanol were used for the ethyl esterification reaction. Mixture 1 represents the reactants at the start of the reaction, where conversion of linoleic acid to ester is 0%. A molar ratio of alcohol to fatty acid of 20:1 was used based on the ratio that was used in actual experiments in this study (Chapter 6). The moles of alcohol were held constant in the formulation for each mixture because it was assumed that the change in the excess alcohol over the course of the

reaction was negligible. A triplicate set of the solutions was formulated to monitor the reproducibility of the method. Figure 20 shows the Raman spectra of the mixtures representing the progression of the ethyl esterification reaction. The mixtures for methyl esterification exhibited a similar peak pattern.

Table 6. Standard mixtures of linoleic acid, ester, and alcohol.

Component	Mixture 1 0% conversion	Mixture 2 25% conversion	Mixture 3 50% conversion	Mixture 4 75% conversion	Mixture 5 100% conversion
Linoleic acid	1 mole	0.25 mole	0.5 mole	0.75 mole	N/A
Ester	N/A	0.75 mole	0.5 mole	0.25 mole	1 mole
Alcohol	20 moles	20 moles	20 moles	20 moles	20 moles
TOTAL	21 moles	21 moles	21 moles	21 moles	21 moles

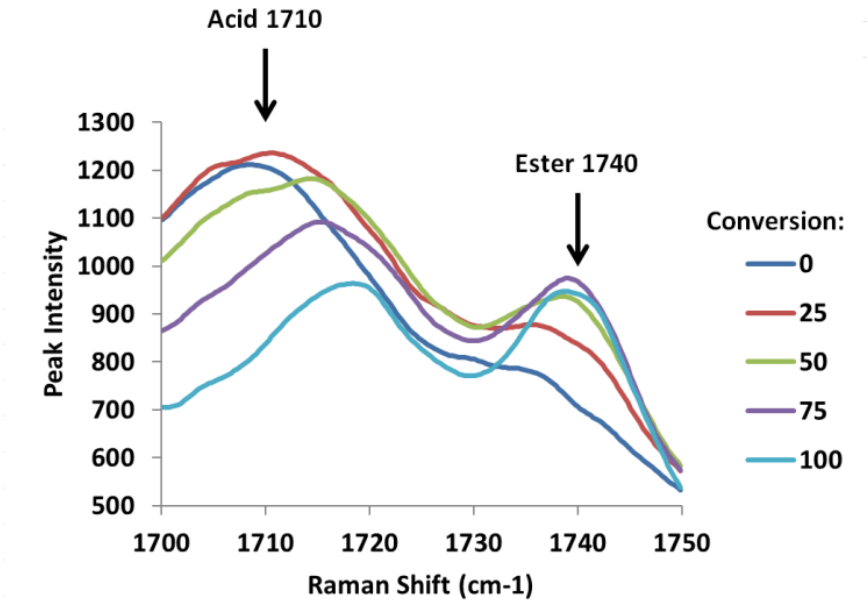

Figure 20. Raman spectra of standard solutions of ethanol, ethyl linoleate, and linoleic acid. The molar ratio of ethanol to a mixture of ethyl linoleate and linoleic acid was constant for each solution at 20:1.

A peak at 1710 cm^{-1} can be seen to decrease as acid concentration decreases. This peak refers to the hydrogen-bonded carboxyl C=O group on the linoleic acid.[69] The excess alcohol interacts with the carbonyl group resulting in alcohol-carbonyl bonding. This was verified by comparison to the additive spectra of the pure reactants. The 1710 cm^{-1} peak does not appear when adding the spectra of linoleic acid and alcohol together.

The reactive peak at 1740 cm^{-1} is attributed to the C=O functional group in the ester.[69] As ester concentration increases, this peak increases. A linear calibration curve was developed using a constant wavelength method to account for the shift of these peaks as their concentrations varied. The intensity ratio, calculated as the intensity of the ester peak divided by the sum of the intensities of the acid and ester peaks, was plotted against conversion to obtain the calibration curves for methyl and ethyl esterification, shown in Figure 21 and Figure 22.

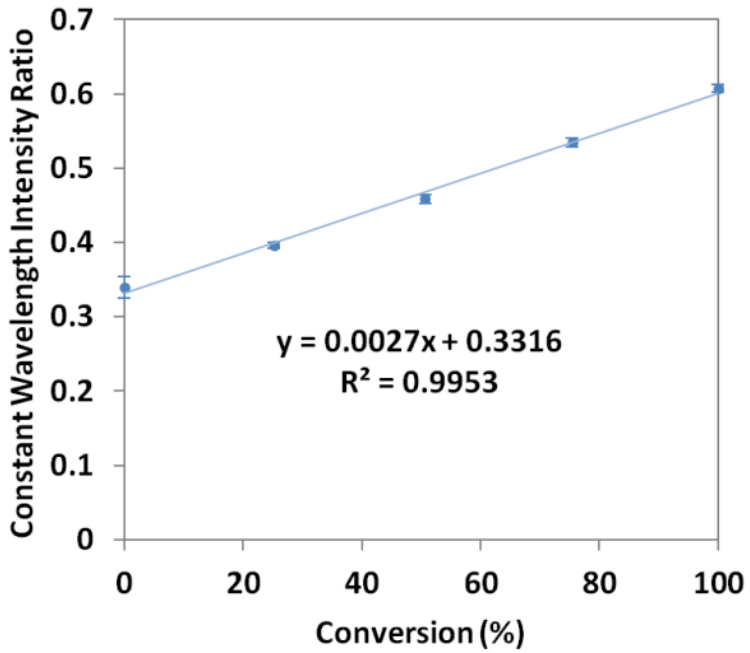

Figure 21. Calibration curve for the Raman spectroscopic analysis of methyl esterification reaction products.

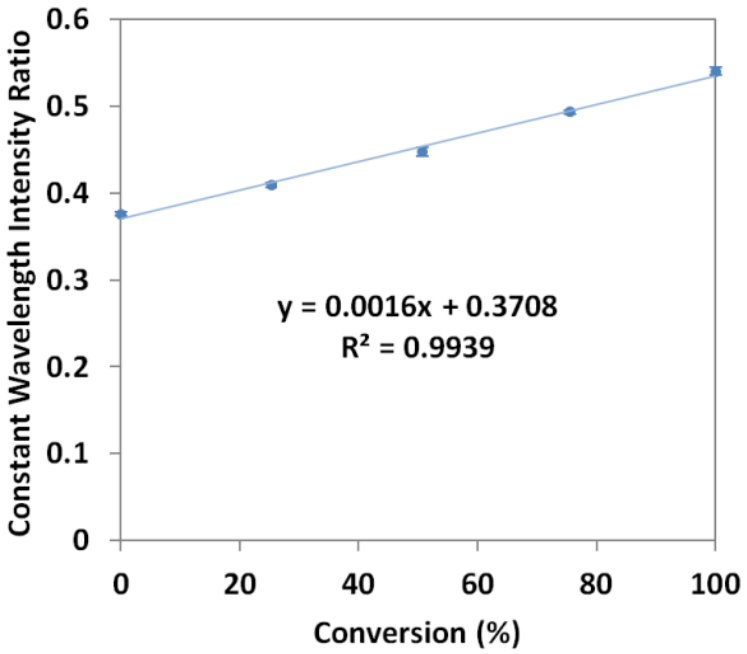

Figure 22. Calibration curve for the Raman spectroscopic analysis of ethyl esterification reaction products.

The coefficients of determination (R^2) for both calibration curves indicate that there is a good correlation between the intensity ratios and conversions. The method proved to be repeatable and reproducible through the use of multiple sets of standard solutions. The calibration curves were then verified by estimating the conversions of samples of known concentrations, shown in Figure 23 and Figure 24.

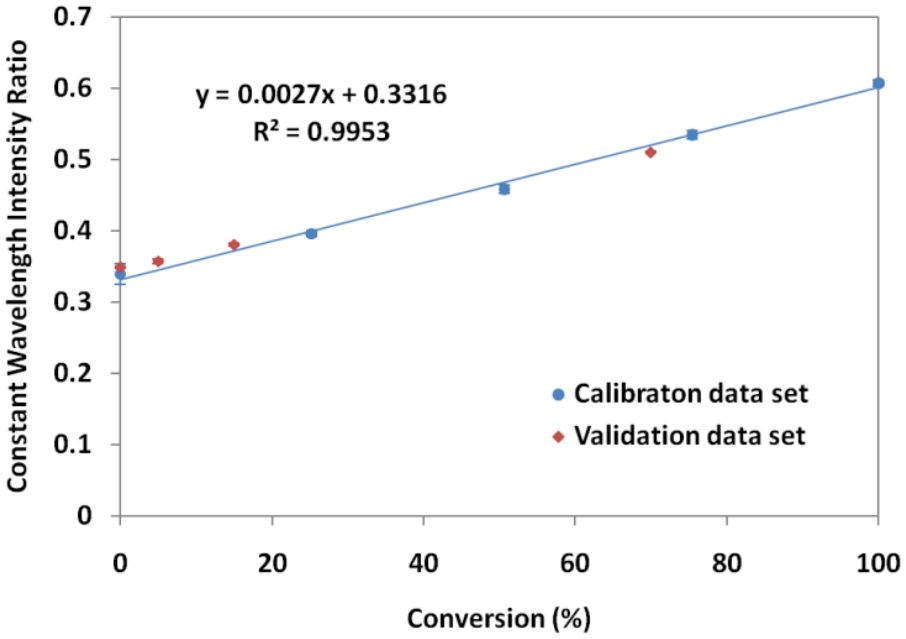

Figure 23. Validation of the calibration curve for methyl esterification.

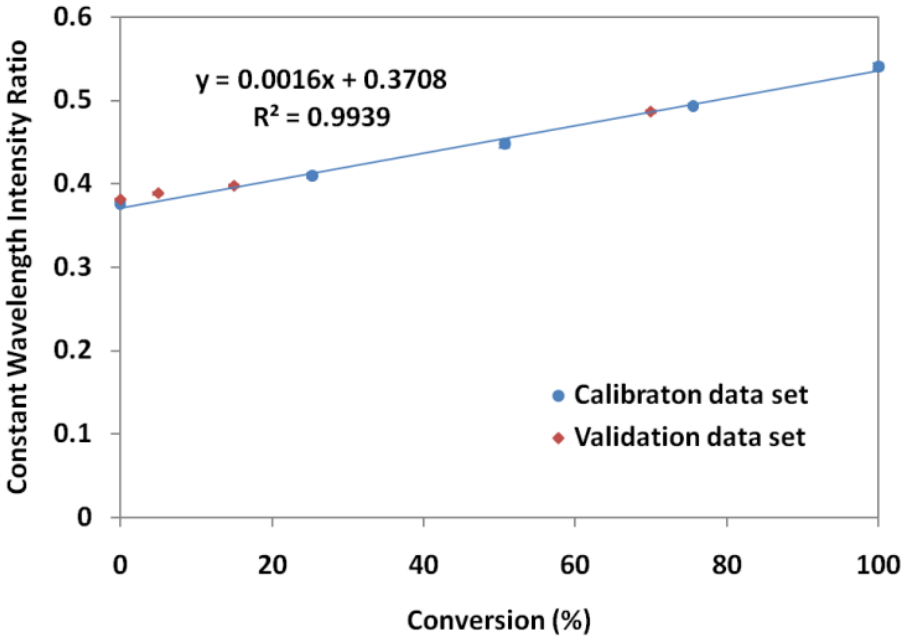

Figure 24. Validation of the calibration curve for ethyl esterification.

Table 7 summarizes the predicted conversions of the known samples, including standard errors that were calculated using the "calibration curve error" equation.[70] This equation takes into account the correlated uncertainties of the slope and the y-intercept (covariance) in the propagation of uncertainty.[71] It can be seen that the calibration is essentially good for conversions above 5%. At low conversions, the signal-to-noise ratio is very low. The 1740 cm^{-1} peak is fundamentally zero at 0% conversion but will read a non-zero number due to the noise in the baseline.

Table 7. Predicted percent conversions of known samples from the use of the methyl and ethyl esterification calibration curves (errors are standard error).

Calibration curve	**Known sample 1 0% conversion**	**Known sample 2 5% conversion**	**Known sample 3 15% conversion**	**Known sample 4 70% conversion**
Methyl esterification	6 ± 3%	10 ± 3%	18 ± 3%	66 ± 2%
Ethyl esterification	6 ± 3%	11 ± 3%	16 ± 3%	70 ± 3%

5.3. Summary

A Raman spectroscopic method was developed for the analysis of methyl and ethyl esterification reaction products. The samples did not require any pretreatment before analysis and data could be collected in seconds. A calibration curve to determine reaction conversion from spectral data was developed and verified to be accurate to within 3% conversion. This non-destructive analytical method could have potential application in in-line reaction monitoring.

CHAPTER 6
EXPERIMENTAL STUDY OF ESTERIFICATION REACTIONS IN A BATCH REACTOR

As mentioned in Chapter 4, the plug flow reactor system became unavailable for all experiments. Thus, a batch reactor system was used to study the kinetics of the esterification reaction. It is important to understand the reaction mechanism and the effects of different reaction conditions in order to effectively design a scaled-up reactor.

Two different alcohols were studied: 1) methanol, and 2) ethanol. Methanol was used because of its current use in the biodiesel industry due to its low cost, while ethanol was selected for use in this study because it is a green solvent (i.e., it is derived from biorenewable resources). Additionally, the batch reactors used in this study were made of quartz. The use of quartz allowed for the elimination of any potential reactive effects from the surfaces of metal reactors.

6.1. Materials and Methods

6.1.1. Materials

Linoleic acid (Sigma-Aldrich, St. Louis, MO) was used as a model compound to represent the free fatty acids in soybean oil, the major biodiesel crop grown in Iowa. Methanol (Fisher Scientific, Fair Lawn, NJ) and ethanol (AAPER Alcohol and Chemical Co., Shelbyville, KY) were used as received. Fused quartz reaction tubes (2 mm I.D. × 6 mm O.D. × 305 mm length) were ordered from Technical Glass Products (Snoqualmie, WA).

6.1.2. Experimental Method

A molar ratio of alcohol to fatty acid of 20:1 (6.7:1 stoichiometric ratio) was used for all experiments. This was based on the ratio used by Silva et al.[26] in their work on the sub- and supercritical transesterification of soybean oil in ethanol so that the kinetics of

both reactions can be compared subsequently. The reaction tubes were charged with the reactants under anaerobic conditions so that oxygen would not be present to create any potential side products. The tubes were only filled one-third full to allow for pressure increases in the system because the reaction pressure could not be monitored.

After the tubes were flame sealed, they were placed in a fluidized bath (Techne Inc., Burlington, NJ) at the desired reaction temperature for various reaction times. Experiments were conducted under the following conditions:

- Reaction temperatures: 250 °C, 270 °C, 290 °C, and 310 °C
- Reaction times: 1, 2, 3, 4, 5, 6, 8, 10, 20, 30, and 1440 minutes

The reaction temperatures were above the critical points of the solvents used. Also, short reaction times (<10 min) were investigated since little information exists on the reaction conversion in this time range. Additionally, experiments were carried out for 1440 minutes (24 hours) to obtain the equilibrium conversion.

The reactions were quenched by immediately transferring the tubes to a water bath. The reaction products were then analyzed using Raman spectroscopy as described in the following section.

6.1.3. Raman Spectroscopy

Raman spectra were collected using an Mk II filtered probehead (Kaiser Optical Systems Inc., Ann Arbor, MI) attached to the HoloLab 5000R modular research Raman spectrograph (Kaiser Optical Systems Inc., Ann Arbor, MI). A 200 mW 785 nm near-infrared laser intensity was delivered to the sample, thereby inducing the Raman scattering effect. Samples were analyzed in a quartz microcuvette (PerkinElmer Inc., Waltham, MA) for an exposure time of 1 second with 3 accumulations. This procedure was carried out in triplicate. All measurements were carried out with auto-dark subtraction and cosmic ray correction. Raman peak height ratios were used to determine conversion by comparison to the calibration curves developed in Chapter 5.

6.2. Results and Discussion

6.2.1. Effects of Temperature, Time, and Alcohol

The effects of temperature and reaction time on the conversion of linoleic acid to methyl and ethyl esters are shown in Figure 25 and Figure 26, respectively. The error bars represent the 95% confidence intervals. The measured conversion at the zero time point yielded a non-zero number due to the low signal-to-noise ratio, as mentioned in the previous chapter.

High conversions could be obtained in short reaction times. The lowest conversion obtained was 47% for the methyl esterification reaction at 250 °C and 1 minute. These conversions were much higher than those of transesterification reactions conducted at the same conditions.[26, 28] As temperature and reaction time increased, conversion also increased.

It was also of interest in this study to conduct experiments at even higher temperatures within the supercritical region (330–350 °C). However, when attempting to perform a reaction at 330 °C, the reaction tube failed. Thus, due to the safety concerns associated with running experiments at such high temperatures in the current setup, the reactions at 330 °C and 350 °C were cancelled from the study plan.

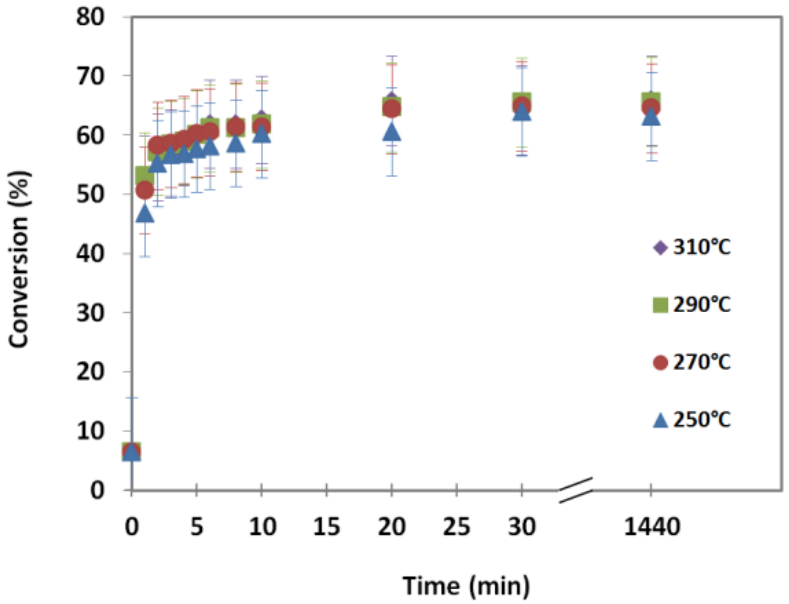

Figure 25. Effect of temperature and reaction time on the conversion to methyl ester. Error bars are 95% confidence intervals.

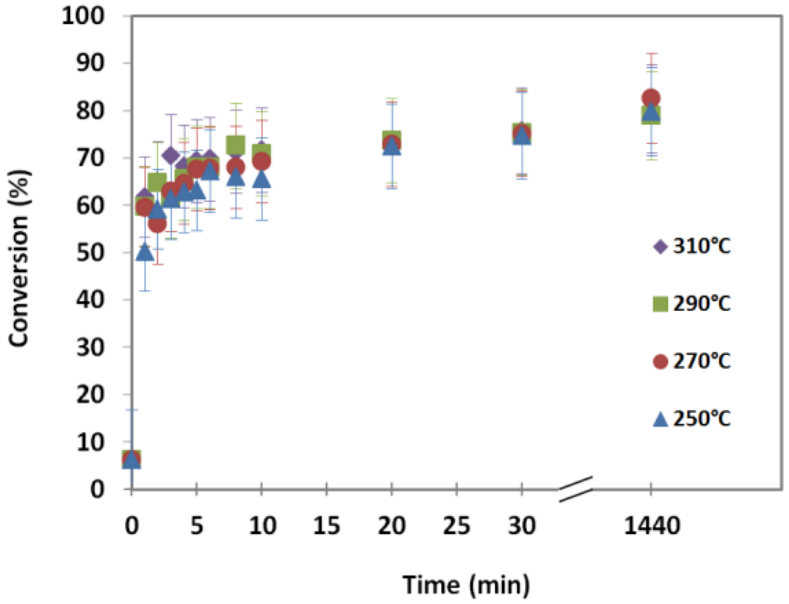

Figure 26. Effect of temperature and reaction time on the conversion to ethyl ester. Error bars are 95% confidence intervals.

It is interesting to note that higher conversions could be observed in the results of ethyl esterification compared to methyl esterification. It was shown by Warabi et al.[31] that alcohols with shorter alkyl groups react faster than alcohols with longer alkyl groups in the transesterification and alkyl esterification reactions. It is possible that the discrepancy of the two data sets in this study is due to experimental uncertainty. It was observed during the analysis of the methyl esterification reaction products that some of the samples were tinted, ranging from a faint to a bright yellow color, possibly caused by the presence of impurities. Despite taking measures to ensure the cleanliness of all the materials used throughout the experiment, it is possible that contamination could have occurred during the transfer of the samples from one vessel to another. The colored samples produced fluorescence that interfered with the Raman spectra, causing the baselines of the spectra to be skewed. In spite of this, the peaks of interest could still be seen in the spectra and since the wavelengths of the peaks were so close together, no modifications were made to the spectra when the peak height ratio was calculated to determine conversion.

6.2.2. Reaction Kinetics

The esterification reaction scheme in Equation 9 was simplified by using variables A, B, C, and D to represent fatty acid, alcohol, ester, and water, respectively:

$$A + B \rightleftarrows C + D \quad (10)$$

Since the reactions were carried out in an isothermal, constant volume batch rector, the differential form of the design equation[72] used in all the kinetic models was:

$$\frac{-dC_A}{dt} = -r_A \quad (11)$$

Namely, the rate of the reaction, $-r_A$, is equal to the change in the concentration of reactant A over time, t. The stoichiometric relationships for this reaction, using A as the basis of calculation, were:

$$C_A = C_{A0}(1 - x) \quad (12)$$

$$C_B = C_{B0} - C_{A0}x \quad (13)$$

$$C_C = C_{A0}x \quad (14)$$

$$C_D = C_{A0}x \quad (15)$$

Where: C_A, C_B, C_C, and C_D are the concentrations A, B, C, and D, respectively; C_{A0} and C_{B0} are the initial concentrations of A and B, respectively, and x is conversion.

Also, Equation 11 in terms of x could be written as:[73]

$$C_{A0}\frac{dx}{dt} = -r_A \quad (16)$$

The equations above were applied to the rate laws of several kinetic models to find the best fit to the data. Each model is discussed in detail in the following sections.

6.2.2.1. Second-Order Forward, Second-Order Reverse

It was first assumed that the esterification reaction follows a reversible reaction model wherein the forward reaction is second order (first order with respect to A and B) and the reverse reaction is also second order (first order with respect to C and D). This assumption was based on previous research that used this model.[50, 51] The rate law for this model is:

$$-r_A = k_f C_A C_B - k_r C_C C_D \quad (17)$$

Where: k_f is the forward reaction rate constant and k_r is the reverse reaction rate constant.

The combined rate law and design equation, written in terms of conversion:

$$C_{A0}\frac{dx}{dt} = -r_A = k_f[C_{A0}(1-x)][C_{B0}-C_{A0}x] - k_r[C_{A0}x][C_{A0}x] \quad (18)$$

was then integrated and rearranged to obtain a function for x in terms of t:

$$x = \frac{\left(e^{t\sqrt{-q}} - 1\right)\left(b^2 + q\right)}{\left(b + \sqrt{-q}\right)\left(2c + 2ce^{\ln\left(\frac{b - \sqrt{-q}}{b + \sqrt{-q}}\right) + t\sqrt{-q}}\right)} \quad (19)$$

Where the constants are defined as follows:

$$q = 4ac - b^2 \quad (20)$$

$$a = k_f C_{B0} \quad (21)$$

$$b = -k_f(C_{A0} + C_{B0}) \quad (22)$$

$$c = (k_f - k_r)C_{B0} \quad (23)$$

Mathcad 15.0 (Parametric Technology Corp., Needham, MA) was used to perform non-linear regression to fit Equation 19 to the data and to obtain the values of k_f and k_r. Figure 27 and Figure 28 show the fit of the model to the data of methyl and ethyl esterification, respectively. The reaction conversion reaches a plateau at longer reaction times. This is probably due to the production of the water co-product that inhibits the formation of ester. Conversion values could potentially increase if water is removed during the reaction.

For methyl esterification, the models for 270 °C and 310 °C seem to overlap each other, indicating that the reaction is independent of temperature. However, this cannot be true because previous research has demonstrated the temperature dependency of the reaction.[48, 51] As mentioned in Section 6.2.1, the conversion data for methyl esterification could be inaccurate due to experimental error.

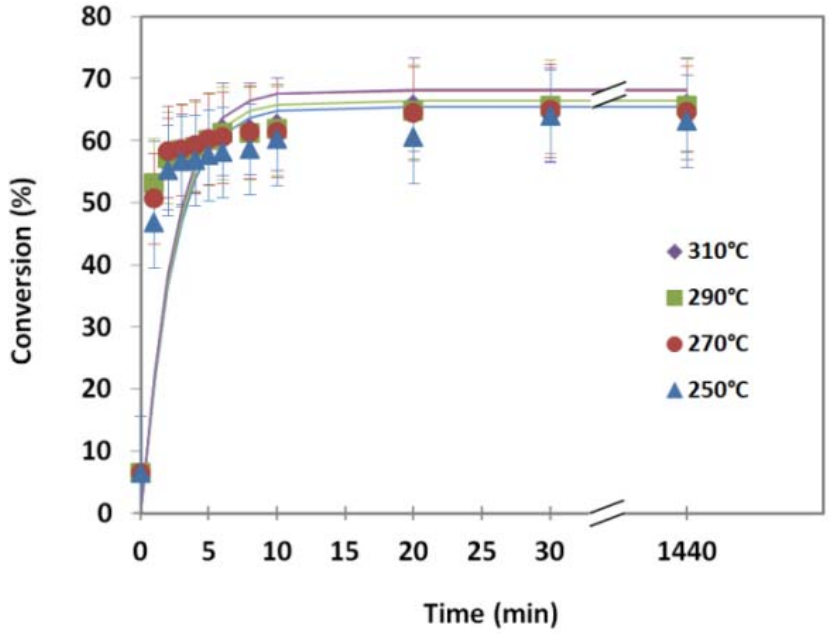

Figure 27. Fit of the second-order forward, second-order reverse reaction model to methyl esterification data. Error bars are 95% confidence intervals.

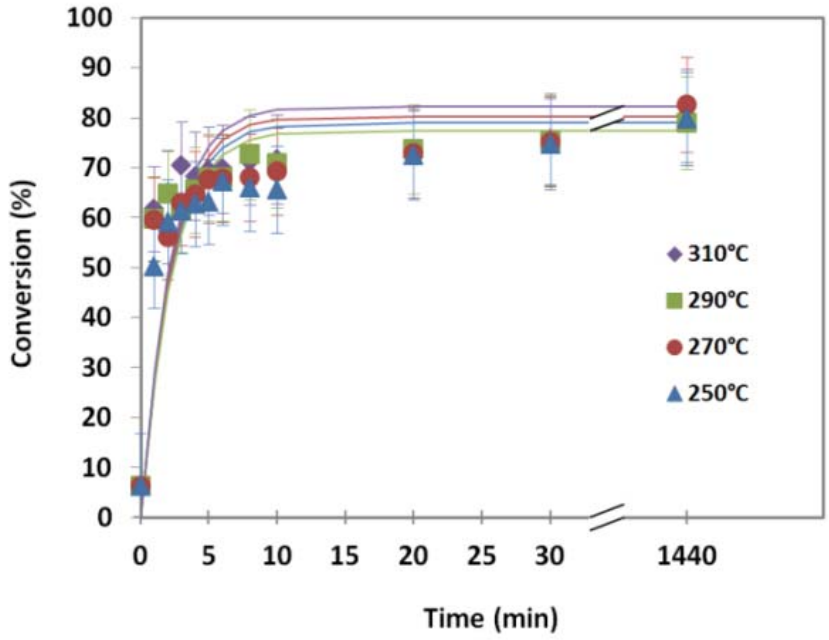

Figure 28. Fit of the second-order forward, second-order reverse reaction model to ethyl esterification data. Error bars are 95% confidence intervals.

Table 8 lists k_f and k_r obtained from this model for both methyl and ethyl esterification. The k values were then used to generate Arrhenius plots to determine the activation energies and the pre-exponential factors. The Arrhenius equation is:

$$k = Ae^{-E_a/RT} \quad (24)$$

Where: k is the rate constant, A is the pre-exponential factor, E_a is the activation energy, R is the gas constant (8.413 J mol^{-1} K^{-1}), and T is temperature.

The equation is linearized:

$$\ln(k) = \ln(A) - \frac{Ea}{R}\left(\frac{1}{T}\right) \quad (25)$$

and ln(k) is plotted against 1/T. Figure 29 and Figure 30 show the Arrhenius plots for methyl and ethyl esterification, respectively. E_a and A obtained from the plots are listed in Table 9.

Table 8. Rate constants from the second-order forward, second-order reverse reaction model.

	Methanol		Ethanol	
Temperature	**k_f (L mol^{-1} min^{-1})**	**k_r (L mol^{-1} min^{-1})**	**k_f (L mol^{-1} min^{-1})**	**k_r (L mol^{-1} min^{-1})**
250 °C	0.014	0.214	0.024	0.159
270 °C	0.015	0.194	0.025	0.147
290 °C	0.014	0.206	0.024	0.171
310 °C	0.015	0.193	0.026	0.131

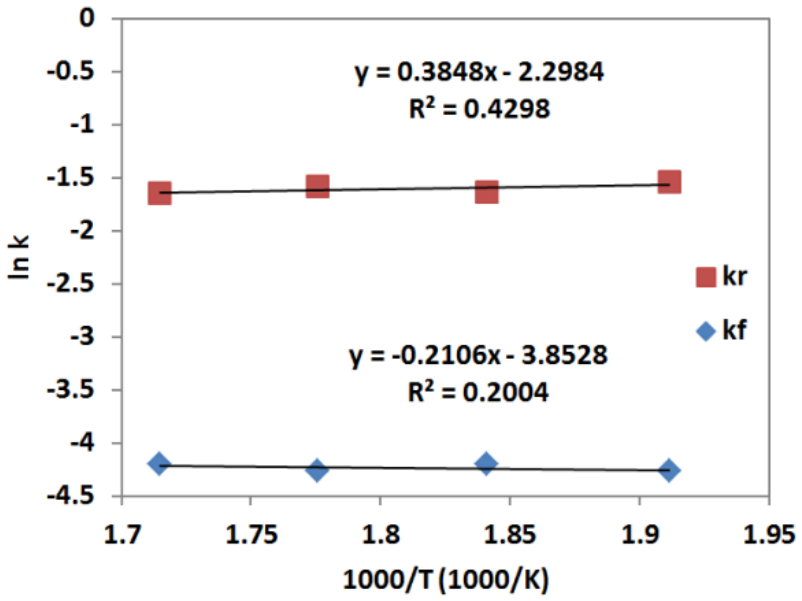

Figure 29. Arrhenius plot for the second-order forward, second-order reverse reaction model for methyl esterification.

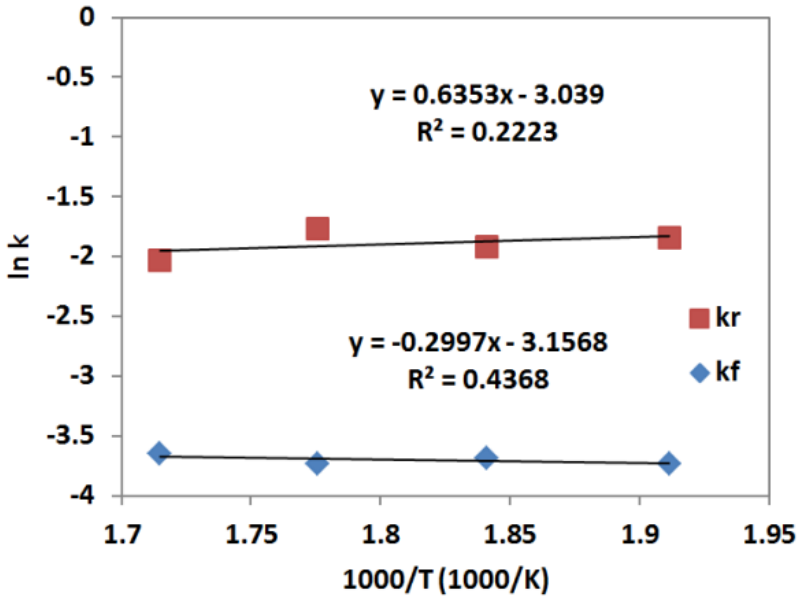

Figure 30. Arrhenius plot for the second-order forward, second-order reverse reaction model for ethyl esterification.

Table 9. Activation energy and pre-exponential factors from the second-order forward, second-order reverse reaction model.

	Methanol		Ethanol	
	Forward reaction	**Reverse reaction**	**Forward reaction**	**Reverse reaction**
E_a (kJ mol^{-1})	2 ± 11	-3 ± 11	3 ± 9	-1 ± 30
Log_{10} A	-2 ± 1	-1 ± 1	-1.4 ± 0.8	-1 ± 3

It can be observed that the reaction rate constants for the reverse reaction are greater than the constants for the forward reaction. This is consistent with the results of Pinnarat and Savage.[50] The forward rate constants were also greater than those calculated for transesterification using a first-order irreversible reaction model,[26] especially at lower temperatures (250–290 °C). Hence, esterification occurs much more quickly than transesterification.

The activation energies of the forward reactions were calculated using the Arrhenius plots and they appeared to be smaller than those reported by Pinnarat and Savage[50] and for homogeneously catalyzed reactions with sulfuric acid.[74, 75] However, the calculation of the activation energies of the reverse reactions yielded negative values which denote a decreasing reaction rate with increasing temperature. Thus, this model does not fit the data and other kinetic models were examined.

The confidence intervals for E_a and A in Table 9 were not included since the curve fitting function in Mathcad did not automatically estimate the errors of the fitted parameters. While the error estimation of non-linear regression parameters can be mathematically complex, Brevington[76] describes a method to obtain these values from an error matrix.

6.2.2.2. Second-Order A Forward, Second-Order Reverse

Since excess alcohol was used in these experiments, it was assumed that the concentration of the alcohol did not affect the forward rate of reaction. It was also assumed that the forward reaction was a second-order reaction with respect to the acid. The rate law for this model is:

$$-r_A = k_f C_A^2 - k_r C_C C_D \quad (26)$$

After combining this rate law with the design equation, it was integrated to obtain a function for x in terms of t. The result took the same forms as Equations 19 and 20 and:

$$a = k_f C_{A0} \quad (27)$$

$$b = -2k_f C_{A0} \quad (28)$$

$$c = (k_f - k_r) C_{A0} \quad (29)$$

As in Section 6.2.2.1, the Mathcad software was used perform non-linear regression to fit this model to the data and obtain the values for the forward and reverse rate constants for both methyl and ethyl esterification. Figure 31 and Figure 32 show the fit of the model to the data. It can be seen that this model fits both reactions similarly to the second-order forward, second-order reverse reaction in the previous section.

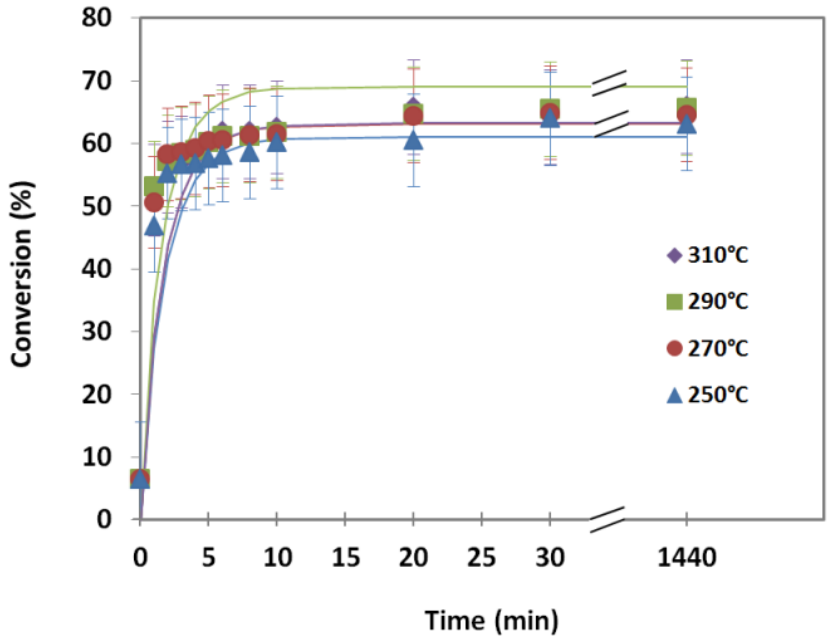

Figure 31. Fit of the second-order A forward, second-order reverse reaction model to methyl esterification data. Error bars are 95% confidence intervals.

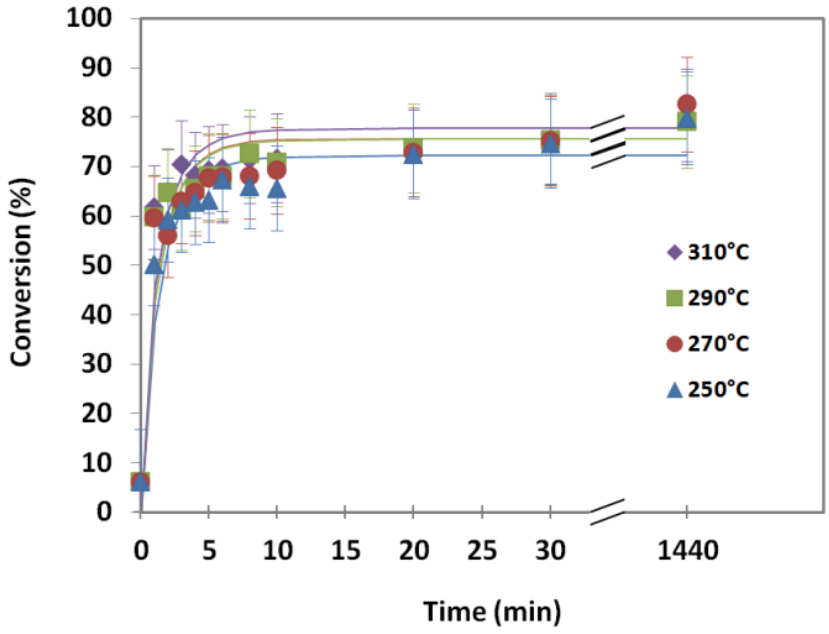

Figure 32. Fit of the second-order A forward, second-order reverse reaction model to ethyl esterification data. Error bars are 95% confidence intervals.

Table 10 lists the k values for both the forward and reverse reactions for methyl and ethyl esterification. The Arrhenius plots are shown in Figure 33 and Figure 34 for methyl and ethyl esterification, respectively. The activation energies and pre-exponential factors obtained from the plots are listed in Table 11.

Table 10. Rate constants from the second-order A forward, second-order reverse reaction model.

	Methanol		Ethanol	
Temperature	**k_f (L mol^{-1} min^{-1})**	**k_r (L mol^{-1} min^{-1})**	**k_f (L mol^{-1} min^{-1})**	**k_r (L mol^{-1} min^{-1})**
250 °C	0.430	0.176	0.941	0.139
270 °C	0.470	0.161	1.131	0.116
290 °C	0.613	0.123	1.120	0.117
310 °C	0.472	0.160	1.259	0.104

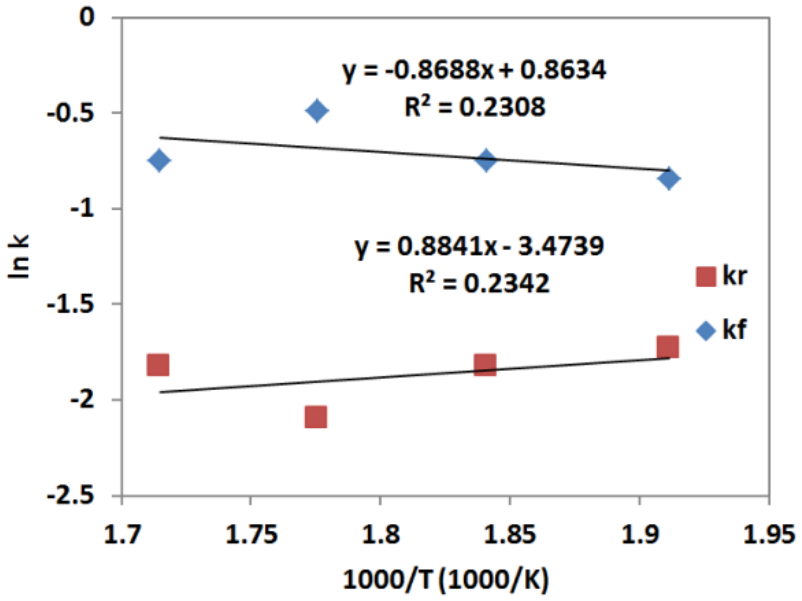

Figure 33. Arrhenius plot for the second-order A forward, second-order reverse reaction model for methyl esterification.

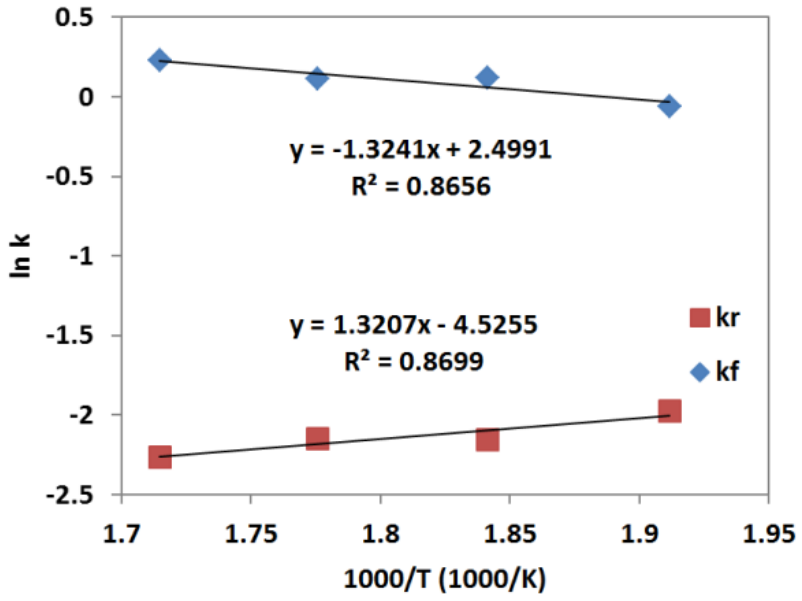

Figure 34. Arrhenius plot for the second-order A forward, second-order reverse reaction model for ethyl esterification.

Table 11. Activation energy and pre-exponential factors from the second-order A forward, second-order reverse reaction model.

	Methanol		Ethanol	
	Forward reaction	**Reverse reaction**	**Forward reaction**	**Reverse reaction**
E_a (kJ mol^{-1})	7 ± 40	-7 ± 40	11 ±13	-11 ±13
Log_{10} A	1 ± 4	-2 ± 4	1 ± 1	-2 ± 1

For this model, the rate constants for the forward reaction are greater than the constants for the reverse reaction. This is consistent with the results of Alenezi et al.[51] However, just as with the model in the previous section, the activation energies of the reverse reaction are also negative, indicating that this model does not fit the data. Again, the confidence intervals of the values in Table 11 were not included because of unavailable error estimates for the fitted parameters, k_f and k_r.

6.2.2.3 Autocatalytic Model

It was also of particular interest to investigate the autocatalytic model proposed by Minami and Saka,[48] wherein the rate law is:

$$-r_A = (k_f C_A C_B - k_r C_C C_D) C_A \qquad (30)$$

However, after combining this rate law with the design equation and performing integration, a function for x in terms of t could not be obtained. Thus, k_f and k_r could not be found using non-linear regression.

An alternative method was used to determine the reaction rate constants of this rate law. It was assumed that equilibrium conversion, x_{eq}, was attained at 1440 minutes so that the equilibrium constant, K_{eq}, could be calculated with the data at that time point. Thus, k_r could be written in terms of k_f and only one variable (k_f) would be computed. K_{eq} was calculated using the following equation:

$$K_{eq} = \frac{C_C C_D}{C_A C_B} \quad (31)$$

where the concentrations, C_A, C_B, C_C, and C_D were previously defined in equations 12, 13, 14, and 15 respectively. Table 12 shows the calculated equilibrium constants.

Table 12. K_{eq} values for the esterification of linoleic acid.

	Methyl esterification	**Ethyl esterification**
Temperature	**K_{eq}**	**K_{eq}**
250 °C	0.055	0.163
270 °C	0.060	0.204
290 °C	0.064	0.154
310 °C	0.065	0.171

The combined rate law and design equation were rearranged in the form of a linear equation:

$$y = mx \quad (31)$$

Where: y is expressed in terms of conversion, m is k_f, and x is time.

A plot of y versus x would yield a straight line and the slope could be obtained, which in turn would yield k_f. The plots for methyl esterification and ethyl esterification are presented in Figure 35 and Figure 36, respectively.

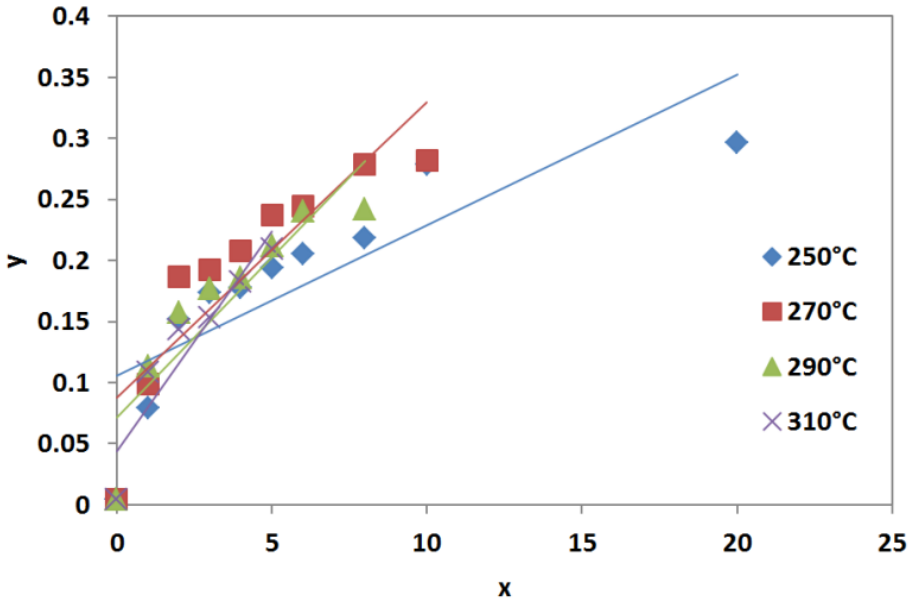

Figure 35. Linearized plots of the autocatalytic model for methyl esterification.

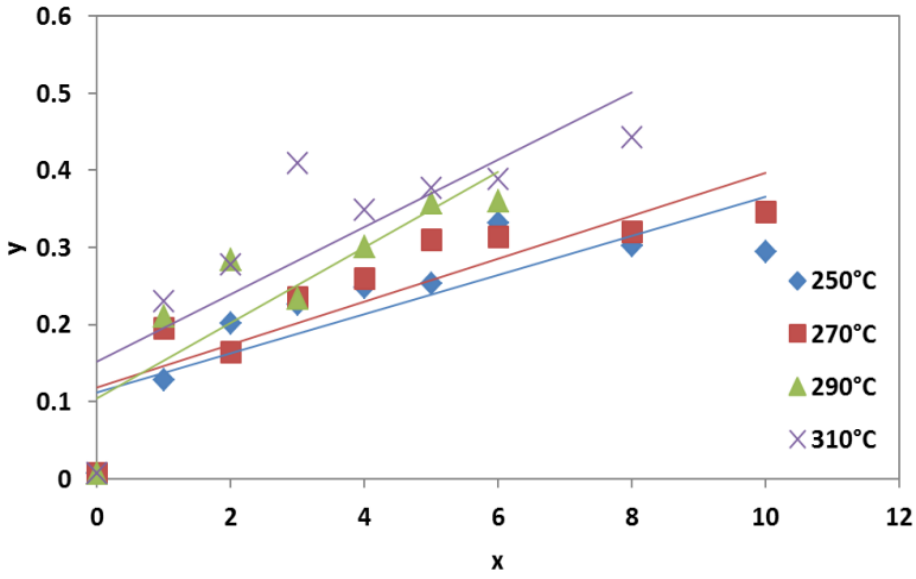

Figure 36. Linearized plots of the autocatalytic method for ethyl esterification.

It appears from the linearized plots that the kinetics model does not fit over the whole range of reaction times. The Arrhenius plots for the autocatalytic model are shown in Figure 37 and Figure 38. The error bars represent the 95% confidence intervals. The activation energies and pre-exponential factors, also with their 95% confidence intervals, are listed in Table 13.

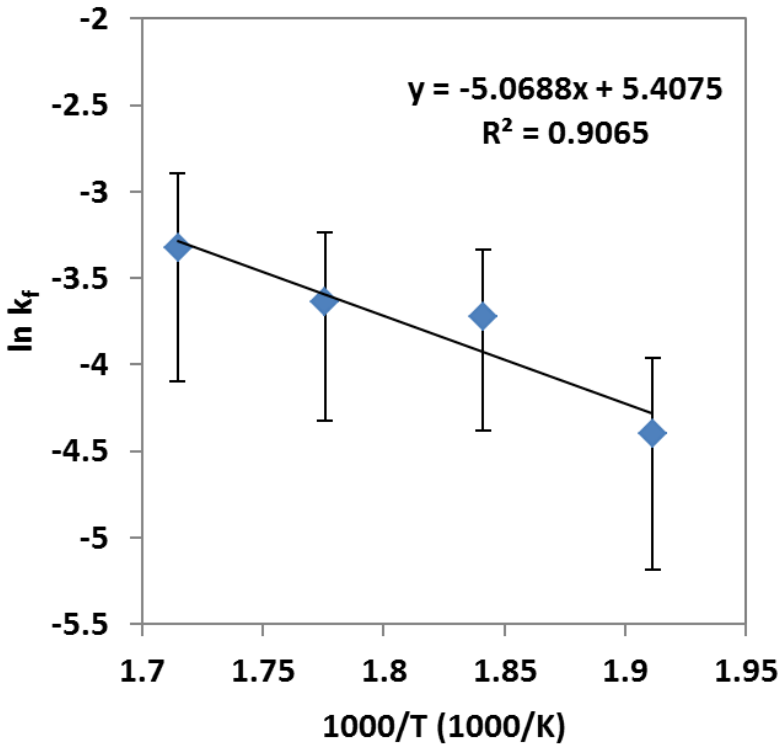

Figure 37. Arrhenius plot for the autocatalytic model for methyl esterification. Error bars are 95% confidence intervals.

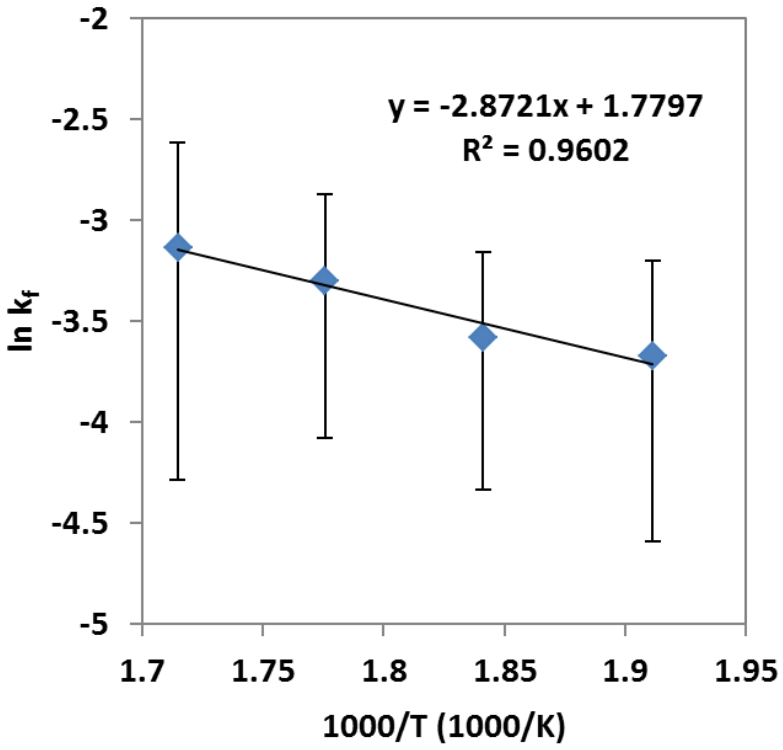

Figure 38. Arrhenius plot for the autocatalytic model for ethyl esterification. Error bars are 95% confidence intervals.

Table 13. Activation energies and pre-exponential factors from the autocatalytic reaction model.

	Methanol	**Ethanol**
	Forward reaction	**Forward reaction**
E_a (kJ mol^{-1})	42 ± 41	24 ± 15
Log_{10} A	2 ± 4	1 ± 1

The Arrhenius plots showed large error bars that indicated large uncertainties in the data. One factor contributing to this large error is the small number of data points (i.e., small number of degrees of freedom). Thus, more data need to be collected at other

temperatures to reduce the uncertainties. Since the Arrhenius plots exhibited such large errors, the values of E_a and A calculated from these plots also showed large errors.

To compare the autocatalytic model to the second-order reversible model in Section 6.2.2.1, the same linearization technique was applied to the second-order reversible model. The linearized plots for methyl esterification and ethyl esterification are shown in Figure 39 and Figure 40. The Arrhenius plots for the linearized second-order reversible model are shown in Figure 41 and Figure 42. The calculated activation energies and pre-exponential factors are shown in Table 14.

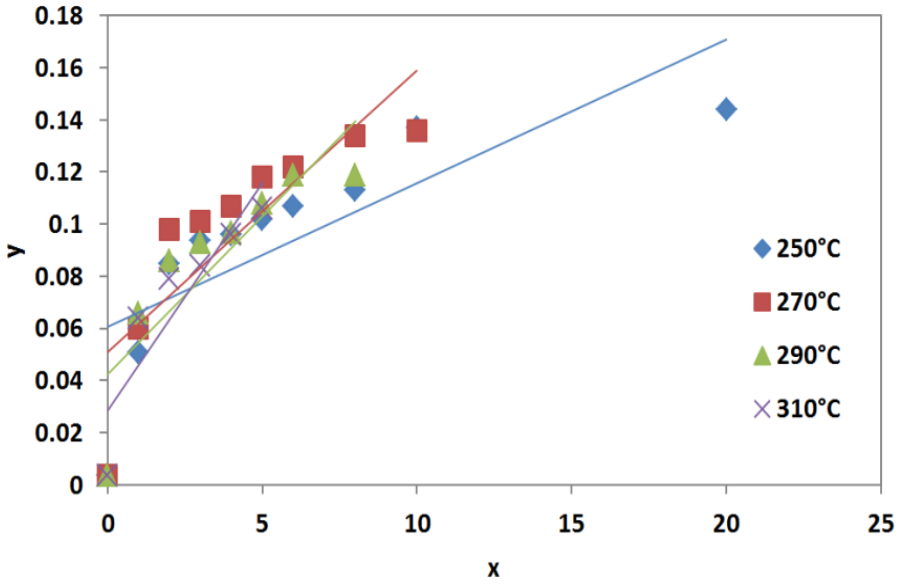

Figure 39. Linearized plots of the second-order reversible model for methyl esterification.

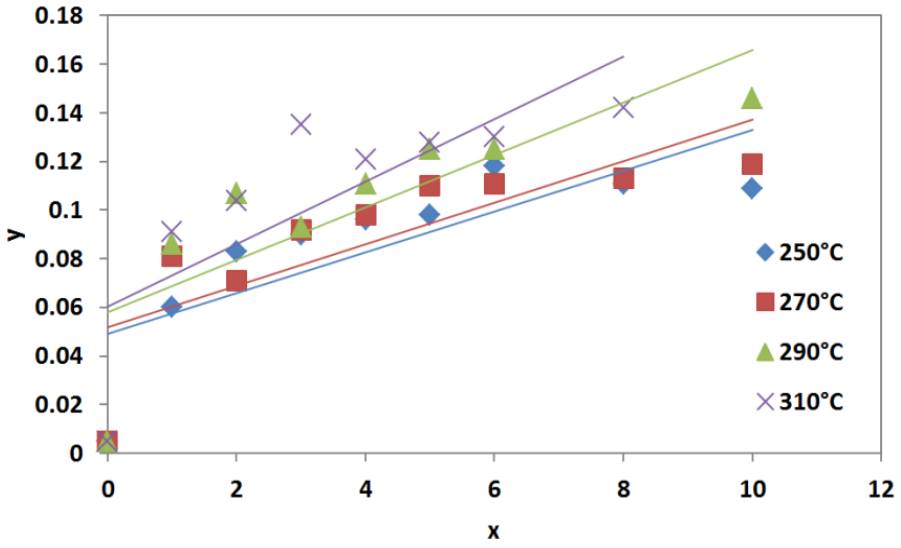

Figure 40. Linearized plots of the second-order reversible model for ethyl esterification.

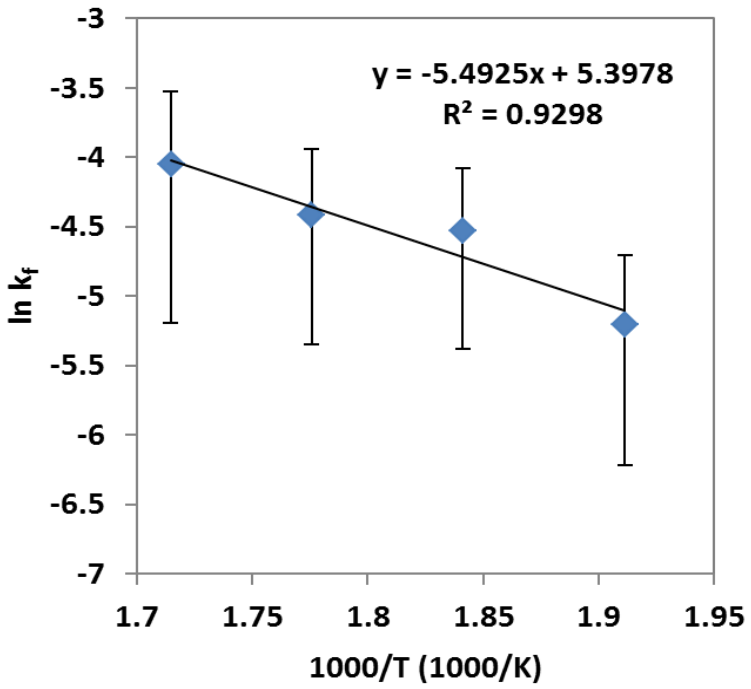

Figure 41. Arrhenius plot for the second-order reversible model for methyl esterification. Error bars are 95% confidence intervals.

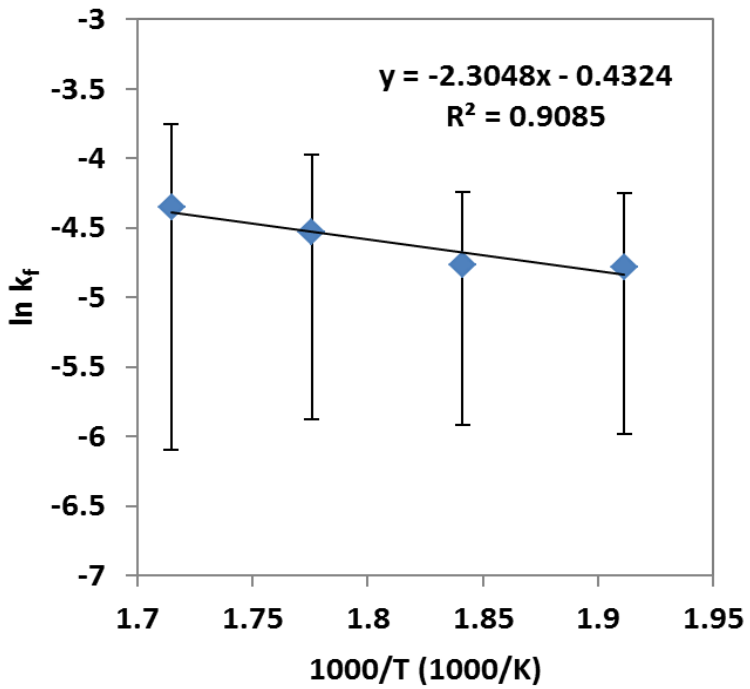

Figure 42. Arrhenius plot for the second-order reversible model for ethyl esterification. Error bars are 95% confidence intervals.

Table 14. E_a and A values from the second-order reversible reaction model.

	Methanol	**Ethanol**
	Forward reaction	**Forward reaction**
E_a (kJ mol^{-1})	46 ± 38	19 ± 18
Log_{10} A	2 ± 4	0 ± 2

The plots of the linearized second-order reversible model yielded similar results to the autocatalytic model. Thus, this model also did not fit over the range of the data. Previous work by Bankole[77] on the esterification of various carboxylic acids, including linoleic acid, using a molar ratio of 1:1 (alcohol to acid) has shown that the second-order reversible model describes the kinetics of this reaction well. Therefore, the results of

these models show that the excess alcohol in the reaction system has significant effects on the kinetics of the reaction.

6.2.2.4. Other Models

Other simplified models were also investigated in this study. Reversible reactions in which the reverse reaction was assumed to be first order yielded results very similar to those obtained from the second-order A forward, second-order reverse model. In one model, it was assumed that the forward reaction was first order in A while in another model, the forward reaction was assumed to be second order in A. Both models generated rate constants that were of the same magnitude as those listed in Table 10. Likewise, their Arrhenius plots exhibited the same trends as those shown in Figure 33 and Figure 34.

Irreversible reaction models, based on the assumption that the excess alcohol drives the reaction forward and prevents the reverse reaction, were also studied. For a reaction that was first order in A, the model did not fit the data as shown in Figure 43 and Figure 44.

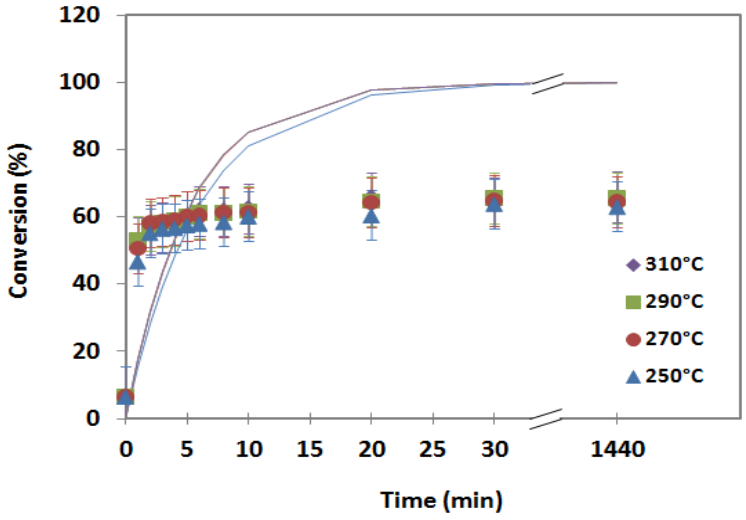

Figure 43. Fit of the first-order A forward reaction model to methyl esterification data. Error bars are 95% confidence intervals.

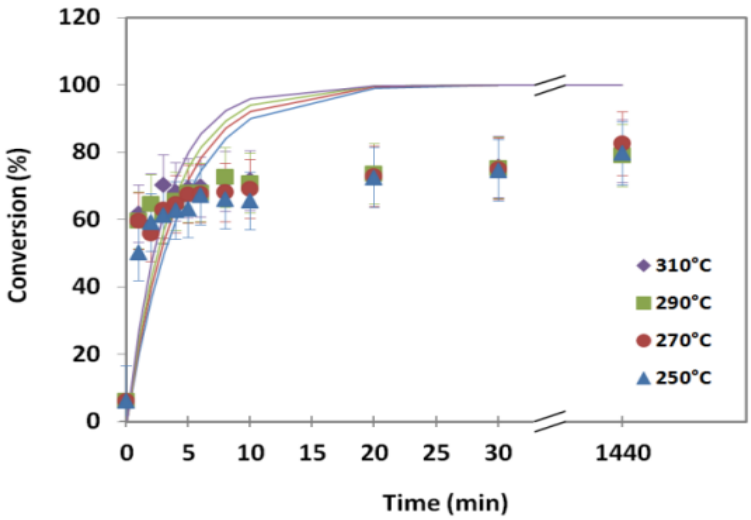

Figure 44. Fit of the first-order A forward reaction model to ethyl esterification data. Error bars are 95% confidence intervals.

Likewise, for an irreversible reaction that was second order in A, the model did not fit the data well and exhibited similar fits to those shown in Figure 43 and Figure 44. Thus, the reverse reaction cannot be neglected in determining a suitable kinetic model for supercritical esterification.

6.2.3. Phase Equilibrium Calculations

Since the pressure inside the reactor tubes could not be monitored during the reaction, it was estimated by performing vapor-liquid equilibrium calculations with the use of ChemCAD (Chemstations, Inc., Houston, TX), a process simulation software. The Predictive Soave-Redlich-Kwong (PSRK) equation was selected for use in the simulations based on Carlson's decision tree for choosing physical property methods for polar, non-electrolyte systems under high pressure.[78]

The algorithm used by Pinnarat and Savage[50] was followed. The experimental density of the system was calculated from the known initial concentrations of the reactants and the volume of the reactor. Temperature, initial moles of the reactants and an

assumed pressure were inputted into the software. The pressure was adjusted until the output density matched the calculated experimental density. The results are shown in Table 15.

Table 15. Estimated pressure of the reaction system.

	Methyl esterification	**Ethyl esterification**
Temperature	**P (bar)**	**P (bar)**
250 °C	76	60
270 °C	98	71
290 °C	127	93
310 °C	155	114

The software also estimated vapor fractions of 1.0 for all the reactions except those at 250 °C. However, it is unclear if this single phase is a vapor phase or a supercritical phase. Reactions at the lowest temperature were predicted to be occurring in a predominantly liquid phase (vapor fraction = 0.2). Future experiments in a view cell would greatly aid in the understanding of the phase behavior of the reaction system at these high temperatures and pressures.

The pressures listed in Table 15 are for a system containing the initial reactants. As the reaction proceeds and products are formed, the composition of the system changes thereby affecting the pressure of the system. Pressure changes over the course of the reaction could have been estimated if the thermodynamic properties of the linoleic acid methyl and ethyl esters were available on ChemCAD.

6.2.4. Discussion

While the autocatalytic model and the second-order reversible models exhibited the better fits to the data among all the kinetic models explored in this study, none of

them fit the data well over the range of reaction temperatures and times studied. Thus, the thermodynamic assumptions in this research need to be reassessed. In this study, ideal solutions were assumed and calculations were simplified with the use of measured concentrations. However, from the results based on this assumption, it is likely that the system is non-ideal.

For non-ideal solutions, the effective concentration of a component, otherwise known as activity, is used instead. It is a function of temperature, pressure, and composition, and it is defined as:[79]

$$a_i(T, P, x) \equiv \frac{f_i(T, P, x)}{f_i(T, P^0, x^0)} \quad (32)$$

where: a is the activity, f is the fugacity, T is temperature, P is pressure, x is the mole fraction. The subscript i indicates the component, and the superscript 0 denotes an arbitrary standard state.

The activity coefficient, a measure of the deviation from ideality, is defined as:

$$\gamma_i = \frac{a_i}{x_i} \quad (33)$$

where: γ is the activity coefficient, a is the activity, x is the mole fraction, and the subscript i indicates the component.

Thus, at equilibrium, the use of activities in the calculation of the equilibrium constant would be better suited to take into account the effects of temperature, pressure, and composition of the system, which the assumption of ideality neglects. ChemCAD, a process simulation software, could be used to estimate equilibrium conversion through the use of its Gibbs reactor module, which minimizes the total Gibbs energy of the

mixture, and the selection of the UNIQUAC activity coefficient model. However, thermodynamic properties for the methyl and ethyl esters of linoleic acid were not available in the software's component database. These properties could be estimated by using methods outlined by Poling et al.[80] and added to the database manually as the starting point for future work.

6.3. Summary

To summarize, high conversions (>50%) for the esterification of linoleic acid were attained for reaction temperatures ranging from 250 °C to 310 °C and reaction times spanning 1 to 30 minutes. It was clearly seen from the data of the ethyl esterification reaction that conversion increased as temperature and reaction time increased. However, this trend was not as clear with the data from the methyl esterification reaction, possibly due to fluorescence interference during Raman data collection.

Equilibrium experiments were conducted for 1440 minutes (24 hours) to obtain the equilibrium conversions, and subsequently the equilibrium constants that were used in determining the reaction kinetics. A second-order reversible model and an autocatalytic model were compared to each other and while they both fit better than models ignoring reversibility, none fit the data well. This could be due to experimental error and the simplified thermodynamic assumption of ideal solutions.

Future work should take into account the non-ideality of these systems at high temperatures and pressures. Furthermore, experiments at times and temperatures beyond the ranges employed in this study will also be required. Additionally, the autocatalytic model should be further investigated using a different method, possibly through the use of an ordinary differential equation solver.

CHAPTER 7

CONCLUSIONS AND RECOMMENDATIONS

To address issues with catalyst use in current biodiesel production technology, non-catalytic methods have been developed. The purpose of this research was to gain a better understanding of non-catalytic hydrolysis and esterification for future reactor scale-up and process design. Another goal was to develop a new analytical method with the potential for in-line reaction monitoring.

Initial experiments in flow reactors were attempted and a continuous flow reactor was successfully designed and assembled. A partial set of data acquired from hydrolysis experiments indicated trends of increasing reaction conversion with increasing temperature, reaction time, and pressure. However, premature equipment failure due to clogging of the back pressure regulator halted the completion of this portion of the work. Future flow reactor designs will need to address this issue. Alternative back pressure valve configurations and manufacturers should be explored, as well as cleaning methods for the reaction system between experiments.

A Raman spectroscopic method was developed for the analysis of esterification reaction products. A calibration curve was generated to extract reaction conversion data from Raman spectra. Reliable data were obtained for ethyl esterification. However, fluorescence interference from impurities in some of the methyl esterification reaction products generated skewed baselines in the spectra and may have caused inaccuracies in the data. The use of an anti-Stokes filter could potentially overcome this fluorescence interference and should be the focus of future work.

Esterification experiments in batch reactor tubes were conducted at temperatures ranging from 250 °C to 310 °C for 1–30 minutes. Additionally, experiments carried out for 1440 minutes (24 hours) were performed to determine the equilibrium conversion that was subsequently used to calculate the equilibrium constant. The integral method was

used to determine which kinetic model best fit the data. The second-order reversible model and the autocatalytic model appeared to fit the data better than other kinetic models that disregarded the reverse reaction. However, none of the models investigated fit the data well.

One reason for the poor fits could be due to experimental error. As mentioned previously, some samples encountered fluorescence interference during collection of the spectral data that may have contributed inaccuracies in the data. Also, despite focusing this study on short reaction times (<10 min), high conversions were already attained at 1 minute. Thus, further experiments at shorter reaction times (<1 min) will be needed to determine which kinetic model fits the data better. This future work could be performed through the use of an enclosed thermally controlled slotted sample cell setup, such as the PerkinElmer Raman Probe – Max (PerkinElmer, Inc., Waltham, MA). It would allow for in situ reaction monitoring of reactions at very short reaction times (on the order of seconds) and it would also prove the in-line monitoring application of the Raman analytical method developed in this research.

Another reason for the poor fits of the models to the data could be the simplified thermodynamic assumption of ideal solutions. The high temperatures and pressures of the reaction system, the hydrogen bonding of the excess alcohol to the linoleic acid (as observed in the 1710 cm^{-1} Raman peak), and the formation of water during the reaction could contribute to the non-ideality of the system. Thus, kinetic modeling that reflects this new assumption of non-ideality should be the focus of future work.

Phase equilibrium calculations were performed using process simulation software to estimate the pressure inside the reaction tubes. Pressures ranged from 60 to 155 bar, increasing as the reaction temperature increased. Furthermore, reactions at 270 °C, 290 °C, and 310 °C were assessed to be occurring in a single phase. However, it was unclear if it was a vapor phase or a supercritical phase. Reactions at 250 °C were two-phase systems that were estimated to be predominantly liquid.

In making a qualitative comparison of the non-catalytic process with the conventional catalyzed process, the advantages and disadvantages of the non-catalytic process are listed in Table 16.

Table 16. Advantages and disadvantages of the non-catalytic production of biodiesel.

Advantages	**Disadvantages**
High conversions in short times	High temperatures and pressures
Not sensitive to feedstock quality	High solvent ratio
No catalyst removal steps	High energy input for solvent removal

With the non-catalytic process, high conversions can be attained much faster than the conventional catalyzed process. No catalyst is used so no refining steps are required to remove it downstream and no waste salts are produced. Also, it is not sensitive to feedstock quality. Thus, cheaper feedstocks, such as waste oils, can be used to lower processing costs.

However, the non-catalytic process does require high energy inputs during reaction and in solvent removal. To optimize this, the heat and solvent streams can be recycled in the process. A comprehensive model simulation that combines the hydrolysis and the esterification reactions will need to be performed, with the aid of process simulation software, to provide an estimation of equipment costs, as well as production costs. This quantitative analysis will aid in identifying the economic benefits of the non-catalytic process.

In conclusion, a novel method using Raman spectroscopy was developed for the analysis of esterification reaction products. This method could potentially be practical in in-line reaction monitoring applications. Also, the thermodynamic assumption of non-ideality should not be neglected in determining which esterification kinetic model best

fits the data. Further experiments at conditions beyond the ranges explored in this study will also be required to clarify the kinetics of the overall reaction. In addition, experiments in flow reactors can provide additional insights about the reaction, but careful consideration of reactor parts is imperative to avoid equipment failure. Furthermore, a more in-depth economic analysis with the use of process simulation software is recommended to determine the cost estimates of this non-catalytic biodiesel production process.

REFERENCES

1. National Biodiesel Board Estimated US Biodiesel Production by Calendar Year. http://www.biodiesel.org/pdf_files/fuelfactsheets/Estimated_Production_Calendar_Years_05-09.ppt (September 30),

2. Schill, S. R. Sizing Up the Soybean Market. http://www.biodieselmagazine.com/article.jsp?article_id=2973 (August 12),

3. National Biodiesel Board Biodiesel FAQs. http://www.biodiesel.org/resources/faqs/ (July 15),

4. Van Gerpen, J., Biodiesel processing and production. *Fuel Processing Technology* **2005,** 86, (10), 1097.

5. Van Gerpen, J.; Shanks, B.; Pruszko, R.; Clements, D.; Knothe, G. *Biodiesel production technology*; National Renewable Energy Laboratory: Golden, CO, 2004.

6. Freedman, B.; Pryde, E.; Mounts, T., Variables affecting the yields of fatty esters from transesterified vegetable oils. *Journal of the American Oil Chemists' Society* **1984,** 61, (10), 1638-1643.

7. Haas, M. J.; McAloon, A. J.; Yee, W. C.; Foglia, T. A., A process model to estimate biodiesel production costs. *Bioresource Technology* **2006,** 97, (4), 671-678.

8. McHugh, M. A.; Krukonis, V. J., Supercritical Fluid Extraction (2nd Edition). In Elsevier: 1994; pp 1-16.

9. O'Neil, A.; Watkins, J. J., Green chemistry in the microelectronics industry. *Green Chemistry* **2004,** 6, (8), 363-368.

10. Krukonis, V., Supercritical Fluids: Their Proliferation in the Pharma Industry. *European Pharmaceutical Contractor* May, 1998, pp 54-59.

11. York, P.; Shekunov, B. Y.; Kompella, U. B., *Supercritical Fluid Technology for Drug Product Development*. M. Dekker: New York, 2004.

12. Duarte, A. R. C.; Mano, J. F.; Reis, R. L., Supercritical fluids in biomedical and tissue engineering applications: a review. *International Materials Reviews* **2009,** 54, (4), 214-222.

13. Peterson, A. A.; Vogel, F.; Lachance, R. P.; Froling, M.; Antal, J. M. J.; Tester, J. W., Thermochemical biofuel production in hydrothermal media: A review of sub- and supercritical water technologies. *Energy & Environmental Science* **2008,** 1, (1), 32-65.

14. Haynes, W. M., *CRC Handbook of Chemistry and Physics* 91st ed.; CRC Press/Taylor and Francis: Boca Raton, FL, Internet Version 2011.

15. Yaws, C. L., Chemical Properties Handbook. In McGraw-Hill: 1999; pp 1-29.

16. Johnston, K., In *Kirk-Othmer Encyclopedia of Chemical Technology*, 3rd ed.; Grayson, M.; Eckroth, D., Eds. John Wiley & Sons: New York, 1984; Vol. Supplement.

17. Jessop, P. G.; Leitner, W., Supercritical Fluids as Media for Chemical Reactions. In *Chemical Synthesis Using Supercritical Fluids*, Jessop, P. G.; Leitner, W., Eds. Wiley-VCH: Weinheim, Germany, 1999; pp 9-13.

18. Diasakou, M.; Louloudi, A.; Papayannakos, N., Kinetics of the non-catalytic transesterification of soybean oil. *Fuel* **1998,** 77, (12), 1297-1302.

19. Pinnarat, T.; Savage, P. E., Assessment of Noncatalytic Biodiesel Synthesis Using Supercritical Reaction Conditions. *Industrial & Engineering Chemistry Research* **2008,** 47, (18), 6801-6808.

20. Saka, S.; Kusdiana, D., Biodiesel fuel from rapeseed oil as prepared in supercritical methanol. *Fuel* **2001,** 80, (2), 225-231.

21. Demirbas, A., Biodiesel from vegetable oils via transesterification in supercritical methanol. *Energy Conversion and Management* **2002,** 43, (17), 2349-2356.

22. Madras, G.; Kolluru, C.; Kumar, R., Synthesis of biodiesel in supercritical fluids. *Fuel* **2004,** 83, (14-15), 2029-2033.

23. Bunyakiat, K.; Makmee, S.; Sawangkeaw, R.; Ngamprasertsith, S., Continuous Production of Biodiesel via Transesterification from Vegetable Oils in Supercritical Methanol. *Energy & Fuels* **2006,** 20, (2), 812-817.

24. He, H.; Sun, S.; Wang, T.; Zhu, S., Transesterification Kinetics of Soybean Oil for Production of Biodiesel in Supercritical Methanol. *Journal of the American Oil Chemists' Society* **2007,** 84, (4), 399-404.

25. He, H.; Wang, T.; Zhu, S., Continuous production of biodiesel fuel from vegetable oil using supercritical methanol process. *Fuel* **2007,** 86, (3), 442-447.

26. Silva, C.; Weschenfelder, T. A.; Rovani, S.; Corazza, F. C.; Corazza, M. L.; Dariva, C.; Oliveira, J. V., Continuous Production of Fatty Acid Ethyl Esters from Soybean Oil in Compressed Ethanol. *Industrial & Engineering Chemistry Research* **2007,** 46, (16), 5304-5309.

27. Demirbas, A., Studies on cottonseed oil biodiesel prepared in non-catalytic SCF conditions. *Bioresource Technology* **2008,** 99, (5), 1125-1130.

28. Kusdiana, D.; Saka, S., Kinetics of transesterification in rapeseed oil to biodiesel fuel as treated in supercritical methanol. *Fuel* **2001,** 80, (5), 693-698.

29. Dasari, M.; Goff, M.; Suppes, G., Noncatalytic alcoholysis kinetics of soybean oil. *Journal of the American Oil Chemists' Society* **2003,** 80, (2), 189-192.

30. Rathore, V.; Madras, G., Synthesis of biodiesel from edible and non-edible oils in supercritical alcohols and enzymatic synthesis in supercritical carbon dioxide. *Fuel* **2007,** 86, (17-18), 2650-2659.

31. Warabi, Y.; Kusdiana, D.; Saka, S., Reactivity of triglycerides and fatty acids of rapeseed oil in supercritical alcohols. *Bioresource Technology* **2004,** 91, (3), 283-287.

32. Kiwjaroun, C.; Tubtimdee, C.; Piumsomboon, P., LCA studies comparing biodiesel synthesized by conventional and supercritical methanol methods. *Journal of Cleaner Production* **2009,** 17, (2), 143-153.

33. Kusdiana, D.; Saka, S., Two-step preparation for catalyst-free biodiesel fuel production. *Applied Biochemistry and Biotechnology* **2004,** 115, (1), 781-791.

34. Tilghman, R. A. Improvement in Processes for Purifying Fatty Bodies. 0011766, 1854.

35. King, J. W.; Holliday, R. L.; List, G. R., Hydrolysis of soybean oil . in a subcritical water flow reactor. *Green Chemistry* **1999,** 1, (6), 261-264.

36. Twitchell, E. Process of Decomposing Fats or Oils into Fatty Acids and Glycerin. 00601603, 1898.

37. Barnebey, H.; Brown, A., Continuous fat splitting plants using the colgate-emery process. *Journal of the American Oil Chemists' Society* **1948,** 25, (3), 95-99.

38. Eisenlohr, G. W. Process of Hydrolyzing Oils and Fats. 02154835, 1939.

39. Chupa, J.; Misner, S.; Sachdev, A.; Smith, G. A., Soap, Fatty Acids, and Synthetic Detergents. In *Kent and Riegel's Handbook of Industrial Chemistry and Biotechnology*, 11 ed.; Kent, J. A., Ed. Springer: New York, NY, 2007; Vol. 2, pp 1694-1741.

40. Bilyk, A.; Bistline, R.; Haas, M.; Feairheller, S., Lipase-catalyzed triglyceride hydrolysis in organic solvent. *Journal of the American Oil Chemists' Society* **1991,** 68, (5), 320-323.

41. Holliday, R. L.; King, J. W.; List, G. R., Hydrolysis of Vegetable Oils in Sub- and Supercritical Water. *Industrial & Engineering Chemistry Research* **1997,** 36, (3), 932-935.

42. Formo, M., Ester reactions of fatty materials. *Journal of the American Oil Chemists' Society* **1954,** 31, (11), 548-559.

43. Sonntag, N., Esterification and interesterification. *Journal of the American Oil Chemists' Society* **1979,** 56, (11), 751A-754A.

44. Johnston, A. C. Method for producing resin acid esters. 01840395, 1932.

45. Butts, D. C. Method for the production of rosin esters. 01979671, 1934.

46. Kaiser, H. E. Method for the continuous production of abietic acid esters. 02074963, 1937.

47. Kusdiana, D.; Saka, S., Methyl Esterification of Free Fatty Acids of Rapeseed Oil as Treated in Supercritical Methanol. *JOURNAL OF CHEMICAL ENGINEERING OF JAPAN* **2001,** 34, (3), 383-387.

48. Minami, E.; Saka, S., Kinetics of hydrolysis and methyl esterification for biodiesel production in two-step supercritical methanol process. *Fuel* **2006,** 85, (17-18), 2479-2483.

49. Petchmala, A.; Yujaroen, D.; Shotipruk, A.; Goto, M.; Sasaki, M., Production methyl esters from palm fatty acids in supercritical methanol. *Chiang Mai Journal of Science* **2008,** 35, (1), 23-28.

50. Pinnarat, T.; Savage, P. E., Noncatalytic esterification of oleic acid in ethanol. *The Journal of Supercritical Fluids* **2010,** 53, (1-3), 53-59.

51. Alenezi, R.; Leeke, G. A.; Winterbottom, J. M.; Santos, R. C. D.; Khan, A. R., Esterification kinetics of free fatty acids with supercritical methanol for biodiesel production. *Energy Conversion and Management* **2010,** 51, (5), 1055-1059.

52. Song, C.; Qi, Y.; Deng, T.; Hou, X.; Qin, Z., Kinetic model for the esterification of oleic acid catalyzed by zinc acetate in subcritical methanol. *Renewable Energy* **2010,** 35, (3), 625-628.

53. Hou, X.; Qi, Y.; Qiao, X.; Wang, G.; Qin, Z.; Wang, J., Lewis acid-catalyzed transesterification and esterification of high free fatty acid oil in subcritical methanol. *Korean Journal of Chemical Engineering* **2007,** 24, (2), 311-313.

54. Petchmala, A.; Laosiripojana, N.; Jongsomjit, B.; Goto, M.; Panpranot, J.; Mekasuwandumrong, O.; Shotipruk, A., Transesterification of palm oil and esterification of palm fatty acid in near- and super-critical methanol with SO4-ZrO2 catalysts. *Fuel* **2010,** 89, (9), 2387-2392.

55. Gui, M. M.; Lee, K. T.; Bhatia, S., Supercritical ethanol technology for the production of biodiesel: Process optimization studies. *The Journal of Supercritical Fluids* **2009,** 49, (2), 286-292.

56. Warabi, Y.; Kusdiana, D.; Saka, S., Biodiesel fuel from vegetable oil by various supercritical alcohols. *Applied Biochemistry and Biotechnology* **2004,** 115, (1-3), 793-801.

57. Knothe, G., Analyzing biodiesel: standards and other methods. *Journal of the American Oil Chemists' Society* **2006,** 83, (10), 823-833.

58. Monteiro, M. R.; Ambrozin, A. R. P.; Lião, L. M.; Ferreira, A. G., Critical review on analytical methods for biodiesel characterization. *Talanta* **2008,** 77, (2), 593-605.

59. Kim, H. J.; Kang, B. S.; Kim, M. J.; Kim, D. K.; Lee, J. S.; Lee, K. Y., Development of heterogeneous catalyst system for esterification of free fatty acid contained in used vegetable oil. In *Carbon Dioxide Utilization for Global Sustainability*, Park, S. E.; Chang, J. S.; Lee, K. W., Eds. Elsevier Science Bv: Amsterdam, 2004; Vol. 153, pp 201-204.

60. Brandao, R. F.; Quirino, R. L.; Mello, V. M.; Tavares, A. P.; Peres, A. C.; Guinhos, F.; Rubim, J. C.; Suarez, P. A. Z., Synthesis, Characterization and use of Nb2O5 based Catalysts in Producing Biofuels by Transesterification, Esterification and Pyrolysis. *Journal of the Brazilian Chemical Society* **2009,** 20, (5), 954-966.

61. A.O.C.S Official Method Cd 3d-63. In *Official methods and recommended practices of the American Oil Chemists' Society*, 4 ed.; Firestone, D., Ed. American Oil Chemists' Society: Champaign, IL, 1989.

62. Stabile, R. G.; Dicks, A. P., Two-Step Semi-Microscale Preparation of a Cinnamate Ester Sunscreen Analog. *Journal of Chemical Education* **2004,** 81, (10), 1488-null.

63. Ghesti, G.; de Macedo, J.; Braga, V.; de Souza, A.; Parente, V.; Figuerêdo, E.; Resck, I.; Dias, J.; Dias, S., Application of raman spectroscopy to monitor and quantify ethyl esters in soybean oil transesterification. *Journal of the American Oil Chemists' Society* **2006,** 83, (7), 597-601.

64. Ghesti, G. F.; de Macedo, J. L.; Resck, I. s. S.; Dias, J. A.; Dias, S. l. C. u. L., FT-Raman Spectroscopy Quantification of Biodiesel in a Progressive Soybean Oil Transesterification Reaction and Its Correlation with 1H NMR Spectroscopy Methods. *Energy & Fuels* **2007,** 21, (5), 2475-2480.

65. Mozharov, S.; Nordon, A.; Girkin, J. M.; Littlejohn, D., Non-invasive analysis in micro-reactors using Raman spectrometry with a specially designed probe. *Lab on a Chip* **2010,** 10, (16), 2101-2107.

66. A.O.C.S Official Method Ca 5-40. In *Official methods and recommended practices of the American Oil Chemists' Society*, 4 ed.; Firestone, D., Ed. American Oil Chemists' Society: Champaign, IL, 1989.

67. Leray, C. TLC Separation of Acylglycerols. http://www.cyberlipid.org/acylglyt/acyl0003.htm (March 11),

68. Leray, C. Thin-Layer Chromatography. http://www.cyberlipid.org/fraction/frac0005.htm (March 11),

69. Lin-Vien, D.; Colthup, N. B.; Fateley, W. G.; Grasselli, J. G., *The handbook of infrared and raman characteristic frequencies of organic molecules*. Academic Press: Boston, 1991.

70. Salter, C., Error Analysis Using the Variance-Covariance Matrix. *Journal of Chemical Education* **2000,** 77, (9), 1239-1243.

71. Harris, D. C., *Quantitative chemical analysis*. W.H. Freeman and Co.: New York, 2003.

72. Fogler, H. S., *Elements of Chemical Reaction Engineering* 4th ed.; Prentice Hall PTR: Upper Saddle River, NJ, 2006.

73. Levenspiel, O., *Chemical Reaction Engineering* 3rd ed.; Wiley: New York, NY, 1999.

74. Aranda, D.; Santos, R.; Tapanes, N.; Ramos, A.; Antunes, O., Acid-Catalyzed Homogeneous Esterification Reaction for Biodiesel Production from Palm Fatty Acids. *Catalysis Letters* **2008,** 122, (1), 20-25.

75. Berrios, M.; Siles, J.; Martín, M. A.; Martín, A., A kinetic study of the esterification of free fatty acids (FFA) in sunflower oil. *Fuel* **2007,** 86, (15), 2383-2388.

76. Bevington, P. R., *Data reduction and error analysis for the physical sciences*. McGraw-Hill: New York, 1969.

77. Bankole, K. S. Uncatalyzed Esterification of Biomass-Derived Carboxylic Acids. Ph.D. dissertation. The University of Iowa, Iowa City, 2011.

78. Carlson, E. C., Don't gamble with physical properties for simulations. *Chemical Engineering Progress* **1996,** 92, (10), 35-46.

79. Prausnitz, J. M.; Lichtenthaler, R. N.; Azevedo, E. G. d., *Molecular thermodynamics of fluid-phase equilibria*. Prentice Hall PTR: Upper Saddle River, N.J., 1999.

80. Poling, B. E.; Prausnitz, J. M.; O'Connell, J. P., *The properties of gases and liquids*. McGraw-Hill: New York, 2001.